JGR Oceans

RESEARCH ARTICLE
10.1029/2023JC020062

Evidence of Langmuir Mixing Effects in the Upper Ocean Layer During Tropical Cyclones Using Observations and a Coupled Wave-Ocean Model

Xiaohui Zhou[1,2], Tetsu Hara[1], Isaac Ginis[1], Eric D'Asaro[3], and Brandon G. Reichl[4]

[1]Graduate School of Oceanography, University of Rhode Island, Narragansett, RI, USA, [2]Princeton University, Princeton, NJ, USA, [3]Applied Physics Laboratory and School of Oceanography, University of Washington, Seattle, WA, USA, [4]NOAA Geophysical Fluid Dynamics Laboratory, Princeton, NJ, USA

Key Points:

- Field observations and numerical modeling are combined to study upper ocean responses under five tropical cyclones
- We find two evidences of the Langmuir turbulence, enhanced vertical velocity variance and reduced mean current shear
- Langmuir turbulence is weaker on the left of storm track possibly because drag coefficient is lower due to swell misaligned from wind

Correspondence to:
X. Zhou,
xz8605@princeton.edu

Citation:
Zhou, X., Hara, T., Ginis, I., D'Asaro, E., & Reichl, B. G. (2023). Evidence of Langmuir mixing effects in the upper ocean layer during tropical cyclones using observations and a coupled wave-ocean model. *Journal of Geophysical Research: Oceans*, *128*, e2023JC020062. https://doi.org/10.1029/2023JC020062

Received 23 MAY 2023
Accepted 22 SEP 2023

Abstract Mixing of the ocean beneath tropical cyclones (TC) cools the surface temperature thereby modifying the storm intensity. Modeling studies predict that surface wave forcing through Langmuir turbulence (LT) increases the mixing and cooling and decreases near-surface vertical velocity shear. However, there are very few quantitative observational validations of these model predictions, and the validation efforts are often limited by uncertainties in the drag coefficient (C_d). We combine EM-APEX and Lagrangian float measurements of temperature, salinity, velocity, and vertical turbulent kinetic energy (VKE) from five TCs with a coupled ocean-wave model (Modular Ocean Model 6—WAVEWATCH III) forced by the drag coefficient C_d directly constrained for these storms. On the right-hand of the storms in the northern hemisphere, where wind and waves are nearly aligned, the measured VKE is consistent with predictions of models including LT and 2–3 times higher than predictions without LT. Similarly, vertical shear in the upper 20 m is small, consistent with predictions of LT models and inconsistent with the large shears predicted by models without LT. On the left-hand of the storms, where wind and waves are misaligned, the observed VKE and cooling are reduced compared to those on the right-hand, consistent with the measured decrease in C_d. These results confirm the importance of surface waves for ocean cooling and thus TC intensity, through both C_d and LT effects. However, the model predictions, even with the LT parameterization, underestimate the upper ocean cooling and mixed layer deepening by 20%–30%, suggesting possible deficiency of the existing LT parameterization.

Plain Language Summary Strong wind under tropical cyclones increases wind forcing at the sea surface, enhances upper-ocean currents and turbulence, and brings deep cold water to the sea surface. The resulting cooler sea surface temperature decreases the heat supply to the storm and weakens the storm. Therefore, it is important to understand how the upper ocean responds to tropical cyclone wind in order to improve the storm intensity forecast. In this study, we investigate how ocean surface waves affect such ocean responses by combining field observations and numerical simulations under five tropical cyclones. We find that upper ocean turbulence becomes more intense because of surface waves. Its intensity is strongly dependent on sea states as well as on wind speed. We also find that ocean responses are weaker on the left of the storm track, possibly because wind forcing at the sea surface is reduced when ocean swell direction and wind direction are misaligned.

1. Introduction

The prediction of tropical cyclone (TC) intensity relies on accurate simulations of sea surface temperature and current field (Bender & Ginis, 2000; Emanuel, 1991). During a passage of a tropical cyclone, the sea surface current can exceed 1 m/s, and cooling of the sea surface temperature (SST) can reach 5°C, which usually occurs to the right of the storm track (in the northern hemisphere). The SST cooling is mainly caused by two processes: the vertical turbulent mixing induced by the strong momentum flux into ocean currents, and the upwelling induced entrainment of cooler thermocline water into the upper mixed layer, driven by diverging Ekman transport under cyclonic wind (Chih & Wu, 2020; Ginis, 2002; Zhang et al., 2016). Under the strong wind forcing of a TC, the enhanced vertical turbulent mixing deepens the mixed layer, entrains colder water from below the mixed layer, and reduces the SST, hence causing reduction of sea surface heat and moisture flux. This reduction may in turn decrease the intensity of the TC. Although these are primarily one-dimensional (vertical) mixing processes, the cool-water entrainment under a tropical cyclone can be further enhanced by three-dimensional processes, notably

by upwelling due to Ekman pumping (Yablonsky & Ginis, 2009). Evaporation is another source of surface cooling and resulting reduction of heat and moisture flux, although this is generally a second-order process during strong winds and active entrainment (Ginis, 2002).

Accurate model simulations of these upper ocean responses require a reliable wind stress (drag coefficient) parameterization. In tropical cyclone conditions (approximately $U_{10} > 25$ m/s, where U_{10} is wind speed at 10 m height), previous observations suggest that the drag coefficient C_d varies by at least a factor of 3—roughly from 1.5×10^{-3} to 4.5×10^{-3} with a weak dependence on wind speed (e.g., Bryant & Akbar, 2016; Donelan et al., 2012; Hsu et al., 2019; Powell et al., 2003; Sanford et al., 2011). Although some of this large variability of observed C_d is likely due to difficulties in measuring wind stress in extreme high wind environments, it is also expected that the drag coefficient depends on factors other than U_{10}, such as surface wave conditions (sea states). Thus without addition information on C_d, simulations of the upper ocean response to a particular storm may have significant errors in air-sea momentum flux. Following Sanford et al. (2011) and Hsu et al. (2017), Zhou et al. (2022) have estimated the wind stress and drag coefficient by combining ocean current observations under 5 TCs and coupled ocean-wave model simulations. On the right to rear-right side of the storm, where wind and waves are aligned, the average C_d ranges between 2.0×10^{-3} and 3.0×10^{-3}, and the stress is close to the downwind direction. When the wind and waves are misaligned by more than 45°, as is common on the left to far front-right side of the storm, C_d is reduced and the drag may be significantly rotated from the wind direction. Note that Chen et al. (2022) also suggests misaligned swell contributes to observed lower drag coefficient in the front-right quadrant of Typhoon Mujigae (2015) compared to those in the rear-right quadrant. The reduced drag coefficient by misaligned wind and wave is found not only in tropical cyclone conditions but also in lower wind conditions. Potter et al. (2022) conduct direct flux measurements at a shallow water platform and show that the drag coefficient is significantly reduced by larger wind-wave misalignment under alongshore winds.

Although the upper ocean responses to TCs are mainly controlled by the applied wind stress, they can be further modified by ocean surface waves. In particular, the interaction between the Stokes drift and the Eulerian current vorticity, which is often referred to as the Craik–Leibovich (CL) vortex force (Craik & Leibovich, 1976), enhances turbulence and vertical mixing (Langmuir turbulence), as demonstrated by McWilliams et al. (1997) and many subsequent large-eddy simulation (LES) studies (e.g., Kukulka et al., 2009; Noh et al., 2004; Polton & Belcher, 2007; Reichl, Wang, et al., 2016). The enhancement occurs over the entire mixed layer even if the Stokes drift is confined in a relatively thin surface layer. Because the intensity of the Langmuir turbulence depends on the relative importance of the wind forcing and the wave forcing, it strongly depends on sea states. Therefore, upper ocean mixing parameterizations without explicit sea state dependence [e.g., the existing community standard K-profile parameterization KPP (Large et al., 1994) i.e., tuned to typical conditions and includes the Langmuir turbulence effect averaged over all sea-states] may introduce significant errors, especially where the surface wave field is not in equilibrium with local wind forcing (Fan & Griffies, 2014; Li et al., 2016), which is particularly common under TCs.

The importance of Langmuir turbulence under TCs has been demonstrated by the modeling study of Reichl, Wang, et al. (2016) (hereafter RWHGK). Reichl, Wang, et al. (2016) developed a modified KPP model that includes the explicit sea state-dependent Langmuir turbulence enhancement. The model has been tuned to match the performance of the KPP to equivalent LES results with identical wind and wave forcing, in a wide range of transient wind and wave conditions under tropical cyclones. The study confirmed that the intensity of the Langmuir turbulence is correlated with the turbulent Langmuir number that characterizes the significance of the wave forcing relative to the wind forcing in TC conditions, as suggested by previous studies in more general (non TC) conditions (McWilliams et al., 1997; Harcourt & D'Asaro, 2008; Li et al., 2016; Van Roekel et al., 2012). The study has also demonstrated that the Langmuir turbulence significantly reduces the near surface current shear and current magnitude due to vigorous momentum mixing. Subsequently, Reichl, Ginis, et al. (2016) have introduced the modified KPP parameterization by RWHGK in a coupled ocean-wave model to investigate the impact of sea state-dependent Langmuir turbulence on the three-dimensional upper ocean responses under idealized tropical cyclones. Their results demonstrate that the sea state-dependent Langmuir turbulence parameterization significantly modifies the sea surface cooling patterns. It also modifies upwelling and horizontal advection patterns because the near-surface currents become weaker in areas where the Langmuir turbulence is more intense.

The importance of Langmuir turbulence at moderate wind speeds ($5 \sim 15$ m/s) is well established both theoretically (see above) and observationally (D'Asaro, 2014; Wang et al., 2022; Zheng et al., 2021). Although its

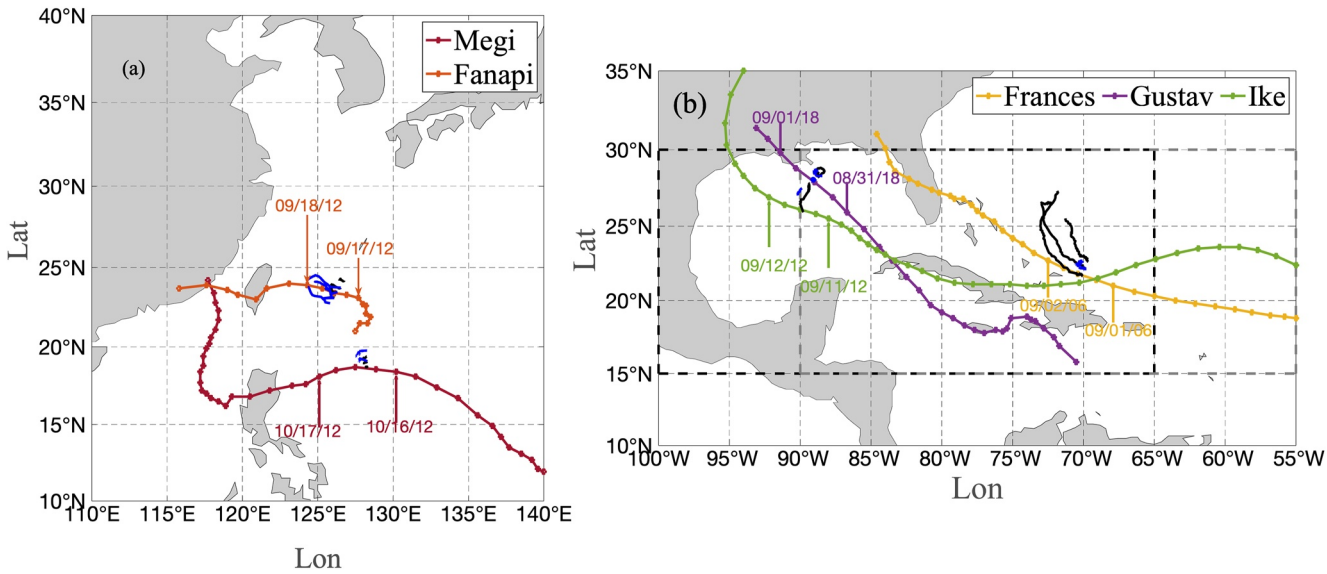

Figure 1. (a) Tracks of Typhoons Megi (red) and Fanapi (dark orange) in Western Pacific. (b) Tracks of Hurricanes Frances (yellow), Gustav (purple), and Ike (green) in North Atlantic and Gulf of Mexico. In both figures colored dots along the tracks show locations every 6 hr, and labels show time (as month/day/hour) 12 hr before and after the storm center was closest to the EM-APEX floats. Black lines indicate the trajectory of EM-APEX floats. Blue lines indicate the trajectory of Lagrangian floats. (These trajectories are shown in more detail in Figure 4.). The spatial domain of MOM6-WW3 for Typhoons is the area shown in (a). The model domain for Hurricane Frances is the gray dashed box in (b). The model domain for Hurricanes Gustav and Ike is the black dashed box in (b).

importance in TC has been demonstrated in modeling studies as discussed above, it has not been quantitatively established by observations. The air-sea interface during TC is significantly different than that at lower winds speeds due to intense wave breaking and spray production that may destroy the smaller surface waves at the highest wind speeds (Holthuijsen et al., 2012). Accordingly, surface wave spectra can have significantly different shapes than those found at lower wind speeds (Hwang et al., 2017). Furthermore, the interaction between Langmuir turbulence and wave breaking, possibly important at lower winds speeds (Sullivan et al., 2007), is likely to be much stronger in TC due to the much stronger wave breaking. Thus, since the physics of the air–sea interface beneath TC is significantly different from that at lower wind speeds, mixing models developed at lower wind speeds need to be validated under TC conditions.

In fact, some previous studies have used field observations to investigate the Langmuir turbulence impacts. Rabe et al. (2015) have investigated the impact of the Langmuir turbulence on the one-dimensional response to Hurricane Gustav (2008), by comparing the observed mixed layer turbulence (vertical velocity variance) and the LES results. Although they find effects of the sea state-dependent Langmuir turbulence, such as enhanced mixed layer cooling, their results are not conclusive because the LES does not consider large-scale three dimensional upper ocean processes and the wind stress (drag coefficient) is not well constrained. Blair et al. (2017) have investigated the sea state-dependent Langmuir turbulence impact on three dimensional ocean responses under Hurricane Edouard (2014), by comparing the field observations (using Airborne Expandable Bathy Thermographs and satellite) and model results (a coupled ocean-wave model with the modified KPP parameterization by RWHGK). They confirm that the effects of sea state-dependent Langmuir turbulence are important especially for mixed layer deepening. However, the uncertainty of wind forcing makes it difficult to assess the accurate surface wave impacts.

In this study, we investigate the impact of Langmuir turbulence on three-dimensional upper ocean responses under TCs, by combining model simulations and field observations and by using wind forcing fields that are well constrained by the upper ocean current observations. This study is motivated by the fact that the importance of Langmuir turbulence, which is well demonstrated by modeling studies, is yet to be quantitatively established by observations in TC conditions. The field observations include EM-APEX float observations of upper ocean currents, temperature, and salinity and Lagrangian float observations of mixed layer vertical velocity variance under 5 TCs—Typhoon Megi (2010), Typhoon Fanapi (2010), Hurricane Frances (2004), Hurricane Gustav (2008), and Hurricane Ike (2008) (Figure 1). The simulations utilize a high resolution coupled ocean-wave model

Table 1
List of EM-APEX Floats and Lagrangian Floats Deployed Under 5 Tropical Cyclones, Including Name, Location of Initial Profiling, and Arrival Time of TC (When the Eye of TC Was Closest to the Float Array)

Tropical cyclone	EM-APEX float	Lagrangian float	Lon(^oE)	Lat(^oN)	Arrival time of TC (t_0)
Frances	*em*1633	*Lag*21/*Lag*22	−69.8	22.1	
	*em*1636		−70.1	21.7	1652 UTC 01-Sep-2004
	*em*1634		−69.7	22.6	
Gustav	*em*3763	*Lag*50	−88.5	28.3	
	*em*3766		−89.3	27.8	0600 UTC 01-Sep-2008
		*Lag*51	−88.9	28.1	
		*Lag*53	−89.7	27.5	
Ike	*em*3766		−89.3	27.8	0030 UTC 12-Sep-2008
Fanapi	*em*4912		126.8	24.2	
	*em*4907	*Lag*60	126.5	23.7	
	*em*4910	*Lag*64	126.3	23.5	2348 UTC 17-Sep-2010
	*em*4906	*Lag*61	126.1	23.1	
	*em*4914*	*Lag*62	126.1	23.1	
Megi	*em*3766		128.3	19.4	
	*em*4913	*Lag*68	128.3	19.1	
	*em*3763		128.3	18.7	2030 UTC 16-Oct-2010
	*em*4911*	*Lag*66/*Lag*67	128.3	19.1	

Note. Most Lagrangian floats were deployed with EM-APEX floats. The * of EM-APEX float denotes that we only used the temperature and salinity profiles to initialize the model simulation.

with different mixing schemes with/without the Langmuir turbulence enhancement. The breaking wave effects on Langmuir turbulence is not considered in the simulations. As discussed earlier, previous studies of the Langmuir turbulence under TCs have not been conclusive because of the large uncertainty of the drag coefficient. To overcome this limitation, in a previous study (Zhou et al., 2022) we estimated the drag coefficient under the same 5 TCs using the same datasets of EM-APEX float current observations and the same wind speed products. One major advantage of this study is that we utilize these wind forcing fields, which are well constrained by the upper ocean current observations, to investigate the Langmuir turbulence.

In this study, we focus on two main objectives: to demonstrate the sea state-dependent enhancement of upper ocean turbulence and mixing due to the Langmuir turbulence, and to assess the overall skill of the KPP mixing scheme that includes the Langmuir turbulence enhancement. We will also investigate the impacts of the reduced drag coefficient in the presence of dominant waves misaligned from wind.

2. Method

2.1. EM-APEX Float and Lagrangian Float Observation

In this study observations from 14 EM-APEX floats and 12 Lagrangian floats deployed under 5 TCs are used, as summarized in Table 1 and shown in Figure 1. One EM-APEX float (float 3766) deployed on the left side of Gustav's track drifted to the right side of Ike's track and provided the measurements under Ike as well (Figure 1). The data from floats 4914 and 4911 are used only for initializing the model temperature and salinity profiles. The deployment time of each EM-APEX float was about 1 day before the storm arrival (Table 1). The 12 Lagrangian floats were usually launched along with EM-APEX floats with the same release from the air deployment package (Table 1, see also D'Asaro, 2003).

The EM-APEX float observations provide the vertical profiles of horizontal current, temperature and salinity roughly every 30 min (Hsu et al., 2017, 2019; Sanford et al., 2011). As discussed by Hsu et al. (2017, 2019) the measured ocean currents include wind driven currents as well as tidal currents and low frequency background

Table 2
List of Maximum Wind Speed V_{max} (m/s), Radius of Maximum Wind R_{max} (km), and Translation Speed (m/s) for Each TC During the EM-APEX Float Observations

Tropical cyclone	V_{max} (m/s)	R_{max}(km)	Translation speed (m/s)
Frances	62	28	6.4~5.4
Gustav	48.7~48	35~45	7.8~6.0
Ike	44~48	75~145	5~5.6
Fanapi	52~62	26~22	3.3~4.2
Megi	62 ~74	16 ~14	8~6.4

currents. Here, the low-frequency background currents are defined as currents that are nearly constant for at least a half day, such as the surface geostrophic currents. Since we compare the observed currents to model simulated currents that are purely wind driven, both the tidal currents and background currents are removed from the measured currents. The storm generated near-inertial oscillations are included in both observed and model simulated wind-driven currents. The full description of extracting wind driven current velocity from the direct EM-APEX velocity measurements is given in Hsu et al. (2017, 2019). EM-APEX floats under Megi and Fanapi did not measure temperature and salinity profiles in the full upper 30 m when wind was too strong. The temperature and salinity profiles under the other three hurricanes were fully measured in the upper 200 m, with a vertical resolution of 1 m.

The Lagrangian floats accurately follow the three dimensional motion of water parcels in the mixed layer by carefully matching their density to that of the surrounding water and by having a large drag (D'Asaro, 2003). The Lagrangian floats can measure vertical velocity from the rate of change of measured pressure as they move inside the mixed layer (D'Asaro et al., 1996; D'Asaro, 2003). Since the floats are Lagrangian, surface wave vertical velocities are naturally filtered out (D'Asaro & Dairiki, 1997; D'Asaro, 2015). The vertical velocities in TC mixed layers are typically 0.03–0.1 m/s and are much larger than the float motion relative to the surrounding water (D'Asaro, Black, et al., 2014; D'Asaro, Thomson, et al., 2014). The smoothed mixed layer averaged vertical velocity variance $< w'^2 >$ is then computed. The detailed description of $< w'^2 >$ calculation can be found in D'Asaro et al. (1996); D'Asaro (2003); D'Asaro et al. (2011); D'Asaro, Black, et al. (2014); D'Asaro, Thomson, et al. (2014); Rabe et al. (2015).

2.2. Wind Fields

Upper ocean model simulations require accurate wind forcing (wind stress) fields, which are difficult to accurately specify under TC conditions. In fact, because of the uncertainty of wind forcing under TCs, the results were not conclusive in the previous attempts to compare field observations and model simulations of upper ocean responses (Blair et al., 2017; Rabe et al., 2015). The uncertainty of wind stress is due to two factors: uncertainty of wind speed, and uncertainty of the drag coefficient.

Zhou et al. (2022) estimated the wind stress by matching the upper ocean current observations (from the EM-APEX floats) and model simulations under the same 5 TCs as in this study. They then estimated the mean drag coefficient based on a particular wind speed product (URI wind in Zhou et al. (2022)) and the estimated wind stress. In this study, we use the same combination of the wind speed product used in Zhou et al. (2022) and the drag coefficient estimated in the their study. Therefore, the wind stress fields applied in our model simulations are consistent with the observed upper ocean current responses, on average over the five TCs. Having this well constrained wind stress field is a major advantage of this study compared to previous studies.

Since the detailed description of the wind speed product (URI wind) is given in Zhou et al. (2022), it is briefly summarized here. First, a symmetric azimuthal wind field is generated by the parametric wind model based on the postseason reanalysis best-track database provided by U.S. Navy Joint Typhoon Warning Center (JTWC) for typhoons and by the National Oceanic and Atmospheric Administration/National Hurricane Center (NOAA/NHC) for hurricanes (HURDAT). The parametric wind model for the two Pacific typhoons is a modified Rankine vortex, while the model for the three Atlantic hurricanes combines a Rankine vortex and a vortex with exponential decay because the Rankine vortex alone overestimates the wind away from the storm center for these hurricanes (Zhou et al., 2022). In order to introduce a radial wind component and asymmetry to the wind field, the inflow angle is specified and 70% of the storm translation speed is added to the wind field as in Moon et al. (2003). Since the parametric wind model does not provide the background wind field away from the storm, we combined the 10-m wind speed field from the Japanese Meteorological Society Reanalysis product (JRA55, Tsujino et al., 2018) with the parametric wind field. Table 2 summarizes the storm parameters (V_{max}, R_{max} and translation speed) of the 5 TCs.

Zhou et al. (2022) estimated the drag coefficient based on the URI wind speed product and the estimated wind stress under the same 5 TCs for $U_{10} \geq 25$ m/s Figure 2 summarizes their wind speed bin averaged drag coefficient.

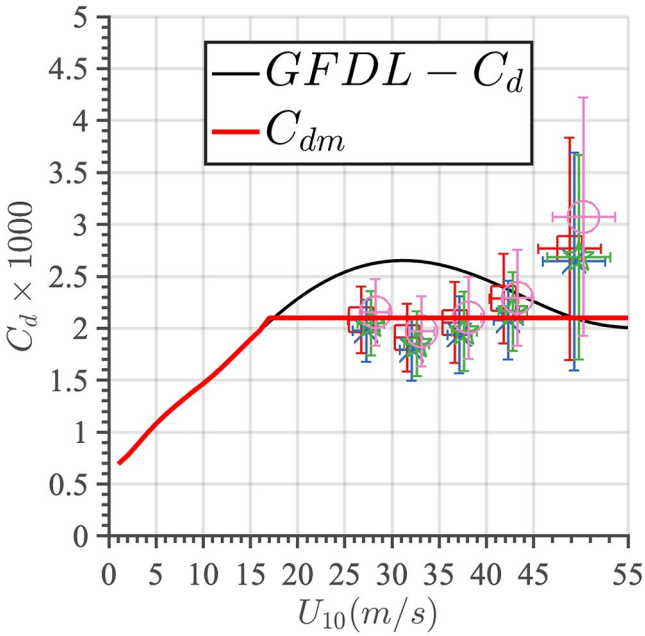

Figure 2. Estimated drag coefficient in Zhou et al. (2022) against U_{10}. Different symbols represent results from four model experiments including different wave effects, see Zhou et al. (2022) for more detail. Horizontal error bars represent the standard deviations of U_{10}. Vertical error bars indicate 95% confidence level. Black line indicates GFDL-C_d. Red line is the parameterization C_{dm} used in this study.

Different symbols represent results from four model experiments with different assumptions regarding surface wave impacts on upper ocean currents (the Langmuir turbulence, the air-sea momentum flux budget, the Stokes advection, the Coriolis-Stokes force, the Stokes-vortex or Stokes shear force). These surface wave impacts can modify the upper ocean current response even if the wind stress forcing is the same. The four model experiments were carried out to investigate the sensitivity of the drag coefficient estimates to different wave impacts. For reference, the black line indicates the drag coefficient implemented in the Geophysical Fluid Dynamics Laboratory (GFDL) hurricane model in 2015 (hereafter GFDL-C_d, Ginis et al., 2015), which produced the best tropical cyclone intensity forecasts using the GFDL and HWRF hurricane models based on a large number of storm simulations (Biswas, 2018; Ginis et al., 2015).

The results of Zhou et al. (2022) show that the dependence of drag coefficient on wind speed is weak in the wind speed range of 25–45 m/s. They also discuss that the uncertainty of the drag coefficient is large for wind speed above 45 m/s (see the large error bars), that is, the apparent increase of the drag coefficient is not reliable. Notice also that the mean C_d values are almost identical from the four model experiments with different assumptions regarding surface wave impacts on upper ocean currents. We therefore simply assume that the drag coefficient is constant at 2.1×10^{-3}, which is the mean value of all the estimations using all four model experiments, when $U_{10} \geq 25$ m/s. We then construct our drag coefficient C_{dm} used in this study (red line in Figure 2), by extending the same constant value to lower wind speeds until it intersects the GFDL-C_d at $U_{10} = 17$ m/s, and then transitioning to the GFDL-C_d for $U_{10} \leq 17$ m/s. Note that all of our subsequent data analyses are performed in high wind conditions of $U_{10} \geq 25$ m/s, which is the same wind range of the drag coefficient estimation of Zhou et al. (2022). Note also that using the GFDL-C_d would significantly overestimate the wind stress and resulting upper ocean current responses, averaged over the five TCs. Zhou et al. (2022) also find that the drag coefficient is sea state-dependent and is significantly reduced when the misalignment between the wind direction and the dominant wave direction exceeds 45°. However, the precise dependence of C_d on the misalignment angle is difficult to constrain because the available observations are limited. Therefore, the sea state dependence of C_d is not introduced in the model simulations of this study.

2.3. Coupled Wave-Ocean Model

The coupled Modular Ocean Model 6—WAVEWATCH III (MOM6-WW3) model is used in this study to simulate the upper ocean responses under TC winds. The MOM6 is the latest version of the modular ocean model with a hybrid vertical coordinate system developed and maintained by NOAA/GFDL (Geophysical Fluid Dynamics Laboratory). For the wave simulation the WW3 version 6.07 is used (WW3DG, 2019). The source terms (ST4) in WW3 are set following Liu et al. (2017) and Chen et al. (2020), which showed good agreement between model results and observations under Hurricane Ivan. In the coupled MOM6-WW3 system, the WW3 provides the dominant wavelength and the vertical profile of the Stokes drift vector to the MOM6. The MOM6 provides the near surface horizontal current vector to the WW3. It is important to introduce the ocean current in the wave model because strong surface currents may significantly decrease the significant wave height under tropical cyclones (Fan et al., 2009).

In MOM6 the following Boussinesq momentum equations (given here in geopotential/height coordinates) are solved (Adcroft et al., 2019):

$$\partial_t u_i + (u_j \partial_j + w\partial_z)u_i + \varepsilon_{i3j} f u_j + \frac{1}{\rho_0}\partial_i p - \frac{1}{\rho_0}\mathcal{F} = 0, \quad i = 1,2;\ j = 1,2 \tag{1}$$

$$\frac{1}{\rho_0}\partial_z p + \frac{\rho}{\rho_0} g = 0 \tag{2}$$

where (u_1, u_2, w) is the (3D) Eulerian velocity, f is the local Coriolis frequency, ρ_0 is the constant Boussinesq reference density, and ρ is the in situ density. In the horizontal momentum equations $\mathcal{F}$ represents the accelerations due to the divergence of stresses (Adcroft et al., 2019). In this study, $\mathcal{F}$ is practically equal to the vertical gradient of the turbulent stress, $\frac{\partial \tau_i}{\partial z}$, because the horizontal stress contribution (the parameterization of unresolved processes such as submesoscale eddies) is much smaller. However, the 3D model is needed because the horizontal advection and pressure gradient terms are not small.

The turbulent stress τ_i is parameterized using the K-Profile Parameterization (KPP) for ocean surface boundary layer mixing via the public CVMix (Community Vertical Mixing) project. We use three different KPP schemes (KPP-ST, KPP-iLT and KPP-LT) proposed by (Reichl, Wang, et al., 2016), who have carefully tuned these KPP schemes against a large number of large eddy simulation (LES) runs under idealized TCs with/without the Langmuir turbulence. These schemes are explained in detail below.

2.4. Experiment Design

Three large computational domains are used for both the ocean and the wave models. As shown in Figure 1, the domain in Western Pacific for Megi and Fanapi ranges 110°E–140°E and 10°N–40°N. The domain in North Atlantic for Frances ranges 90°W–55°W and 15°N–30°N. In Gulf of Mexico, the domain for both Gustav and Ike ranges 100°W–65°W and 15°N–30°N. The spatial resolution is 1/24°, which is around 4.5 km, and the temporal resolution is 300 s for both MOM6 and WW3. The vertical resolution in MOM6 is 4.5 m in the upper 100 m and gradually increases below, which is identical to the vertical levels used in Reichl, Ginis, et al. (2016). This is sufficient to resolve the variation of the mixing layer depth (Reichl, Ginis, et al., 2016). The surface wave spectrum in WW3 is discretized using 48 directions and 40 frequencies. Zhou et al. (2022) summarize comprehensive validations of WW3 simulations under TCs against observations in previous studies (Fan et al., 2009; Liu et al., 2017; Moon et al., 2003). They also validate the WW3 simulated significant wave height using available NDBC buoy observations under Hurricanes Frances and Gustav (see their Figure 8). Their estimated WW3 uncertainties of significant wave height, dominant wave length, and dominant wave direction are about 1 m, 50 m, and 10°, respectively. These are sufficiently small for our calculations of the surface layer averaged Stokes drift (used in Equation 4 and explained in the paragraph following Equation 4), turbulent Langmuir number (defined in Equation 4), and other wave parameters used in this study. For example, when the significant wave height H_S is ∼10 m, uncertainty of ∼1 m (∼10%) of H_S introduces ∼20% uncertainty in the mean square wave elevation, ∼20% uncertainty in the surface layer averaged Stokes drift, and ∼10% uncertainty in the turbulent Langmuir number. These uncertainties do not significantly affect our results and do not change main conclusions of this study. The reason for this is that while shorter surface waves contribute more to the surface layer averaged Stokes drift than to H_S, both quantities are mostly determined by the dominant part of the spectrum and shorter wave contributions are negligibly small.

A separate model experiment is performed for each float initialized from the observed temperature and salinity profiles and a calm (zero currents) ocean condition. The initial temperature and salinity profiles in the model experiment (shown in Figure 3) are prescribed spatially homogeneous. The initial profiles are determined by spatially and temporally averaging the vertical profiles from EM-APEX floats observations before the arrival of TC's eye. The initial mixed layer under Gustav and Ike were shallower because these observations were made in Gulf of Mexico. We use a horizontally homogeneous initial condition because the objective of the model experiment is to accurately simulate "local" upper ocean fields along each float track. All float observations used in this study are made away from regions with strong horizontal gradient, such as the western boundary currents in the Atlantic and Pacific basins and the Loop Current in the Gulf of Mexico. The simulation starts 3 days before the TC center reaches the closest distance to the float and continues for 5 days. This allows us to investigate the upper ocean response during the initial phase, when the wind forcing is weak at the storm periphery, through the strong wind forcing near the storm eyewall, and during the relaxation phase after the storm has passed.

We do not introduce the surface heat and buoyancy fluxes in our simulations, because we focus on the initial wind driven upper ocean responses in this study. Previous studies show that the primary mechanism by which the mixed layer is cooled is entrainment of cooler water from the base of the mixed layer, accounting for over 90% of the total cooling (Price, 1981; Rabe et al., 2015; Sanford et al., 2011; Sullivan et al., 2012). We also note that strong precipitation in the spiral rainbands may impact the upper ocean responses. However, such effects are not included in this study.

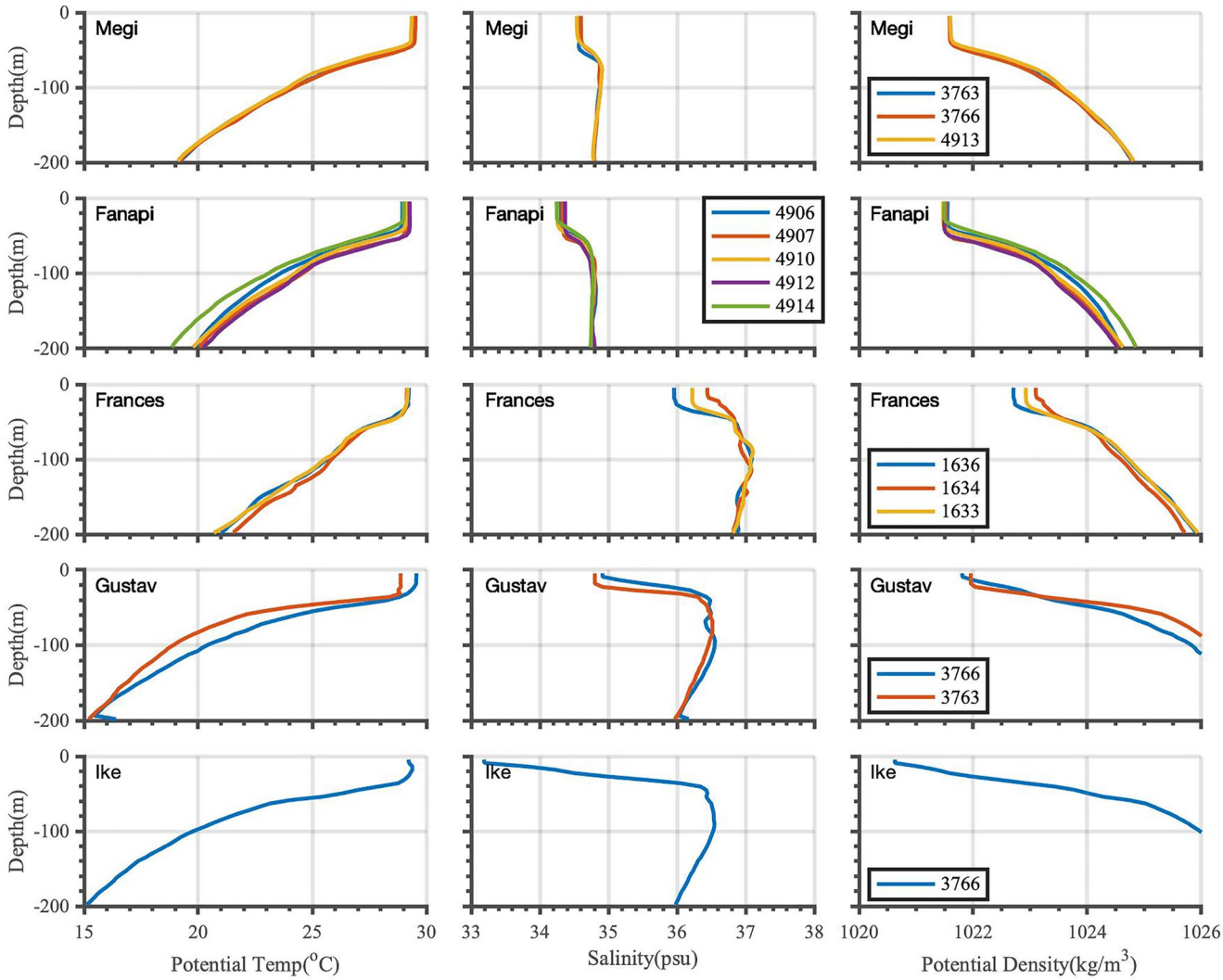

Figure 3. Time averaged vertical profiles of potential temperature (left), salinity (middle), and potential density (right) at each EM-APEX float before the arrival of TC's eye. Different colors indicate different EM-APEX floats under each TC (labeled).

Three experiments using three different KPP mixing schemes are performed to examine the impacts of surface wave induced Langmuir turbulence on the upper ocean responses.

Experiment A is the baseline experiment with no surface wave impacts, and is conducted with the KPP-ST mixing scheme. The KPP-ST mixing scheme is the same as the standard KPP scheme. For the KPP-ST, Ri_{cr} is set 0.27 so that its performance is consistent with the LES results with shear-driven turbulence only (Reichl, Ginis, et al., 2016; Reichl, Wang, et al., 2016).

Experiment B is performed with the implicit (sea state-independent) Langmuir turbulence model (KPP-iLT mixing scheme). The KPP-iLT mixing scheme is also the same as the standard KPP scheme, but the critical Richardson number Ri_c is increased to 0.35 so that it reproduces the LES results with the Langmuir turbulence. This scheme does not depend on sea states. Although the simulated mixed layer deepening using this scheme is reasonably consistent with the LES results on average, it overestimates near surface current shear and surface currents (Reichl, Wang, et al., 2016). Note that both the standard KPP scheme and the KPP-iLT are tuned to typical Langmuir turbulence conditions averaged over all sea states. While the standard KPP is usually tuned to observations in non TC conditions, the KPP-iLT is tuned to LES results in TC conditions.

Experiment C is performed with the explicit (sea state-dependent) Langmuir turbulence model (KPP-LT mixing scheme). Although both KPP-iLT and KPP-LT are tuned to the same set of LES results, the KPP-LT closely

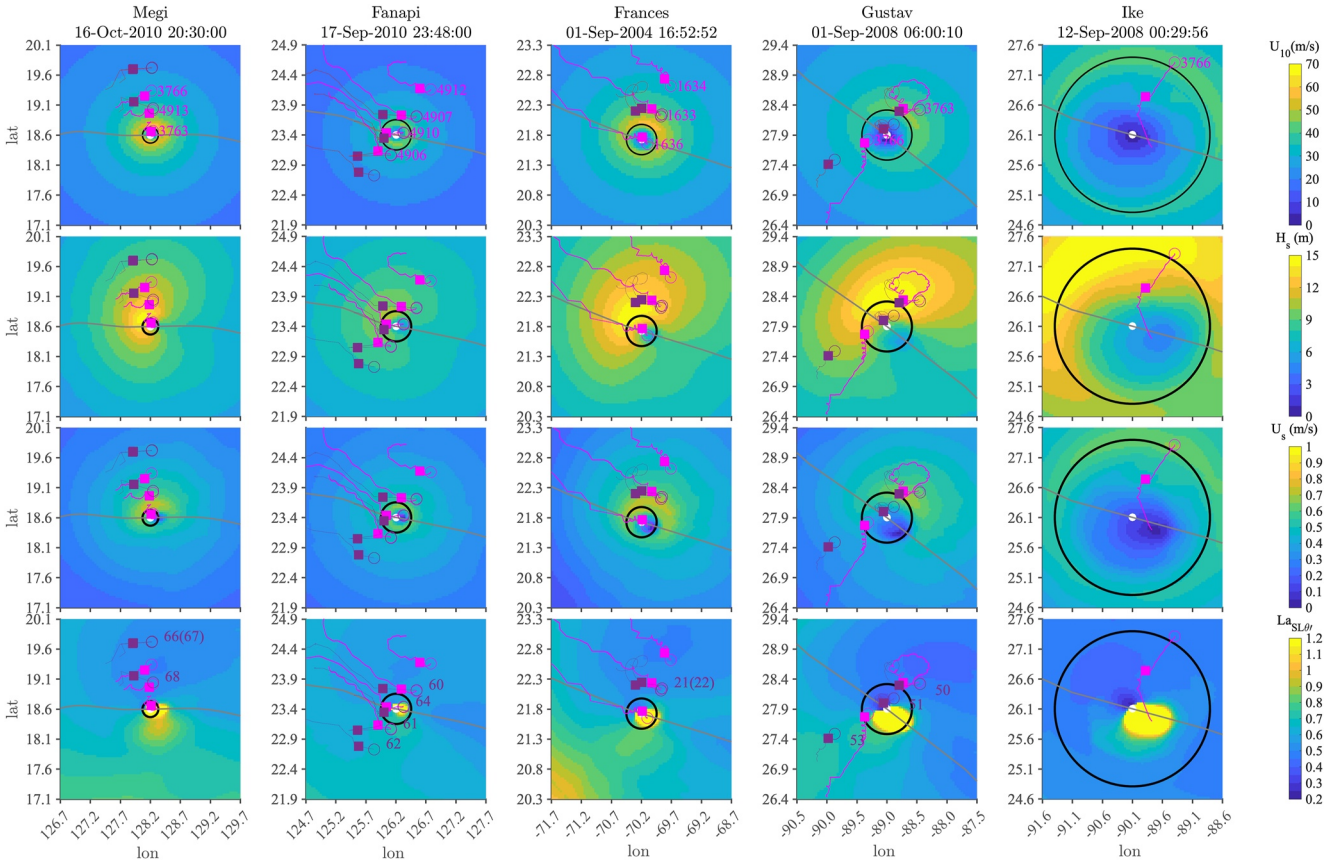

Figure 4. Wind speed (top row), significant wave height (H_s, second row), surface stokes drift (third row) and surface layer averaged turbulent Langmuir number ($La_{SL\theta'}$, bottom row) for 5 tropical cyclones at the time when the storm center was closest to EM-APEX float array (t_0 in Table 1). Gray lines show the trajectory of TCs. Pink lines show trajectories of EM-APEX floats, and purple lines indicate trajectories of Lagrangian floats. The EM-APEX float numbers are labeled on the top panel, and the Lagrangian float numbers are labeled on the bottom panel. White circles represent the storm centers and thick black lines are the radius of maximum wind at the time of snapshot. Pink and purple circles mark the initial location of floats. Pink and purple filled squares mark the location of floats at the time of wind map.

reproduces the sea state dependence of the simulated Langmuir turbulence. In particular, the KPP-LT reproduces the near surface currents more accurately. The KPP-LT differs from the KPP-ST in three ways. First, the turbulent momentum flux is determined by the Lagrangian current shear instead of the Eulerian current shear,

$$\tau_i = -K\frac{\partial u_i^L}{\partial z}, \qquad i = 1, 2 \tag{3}$$

where K is the eddy viscosity and u_i^L is the Lagrangian current, which is a sum of the Eulerian current and Stokes drift.

Second, the KPP-LT model introduces an enhancement factor F_{LT} to the eddy viscosity K, as defined in Reichl, Wang et al. (2016) and Reichl, Ginis, et al. (2016), and F_{LT} is a function of the surface layer averaged turbulent Langmuir number $La_{SL\theta'}$, which is defined (following Van Roekel et al., 2012) as:

$$\mathrm{La}_{\mathrm{SL}\theta'} = \sqrt{\frac{u_*}{\langle|\mathbf{u}^S|\rangle_{\mathrm{SL}}}\frac{1}{\max\left[\cos\left(\theta_{\mathrm{Waves}} - \theta_{\mathrm{Lag}}\right), 10^{-8}\right]}}, \tag{4}$$

where $\mathbf{u}^S$ is the Stoke drift, $\left\langle\left|\mathbf{u}^S\right|\right\rangle_{\mathrm{SL}}$ is the Stokes drift averaged over the surface layer, θ_{waves} is the direction of the Stokes drift averaged over the surface layer, and θ_{Lag} is the direction of the Lagrangian shear averaged over the surface layer. Here, the surface layer is defined as upper 20% of the mixing layer (Harcourt & D'Asaro, 2008; Van Roekel et al., 2012; Reichl, Wang et al., 2016), and the mixing layer is where the bulk Richardson number is smaller than the critical Richardson number ($Ri_b < Ri_c$).

Third, the bulk Richardson number calculation in the KPP-LT model is modified by replacing the Eulerian current with the Lagrangian current, and introducing an enhancement factor $F_{LT}^{V_t}$ to the unresolved turbulent shear contribution V_t^2. Here, $F_{LT}^{V_t}$ is also a function of the surface layer averaged turbulent Langmuir number $La_{SL\theta'}$. More detailed description of the KPP-LT is given in Reichl, Wang, et al. (2016).

Although there are other sea state-dependent Langmuir turbulence mixing schemes, in this study we choose the KPP-LT scheme of Reichl, Wang, et al. (2016) because this is the only mixing scheme that has been developed for high wind tropical cyclone conditions. In fact, Li et al. (2019) have compared performances of 11 existing mixing schemes for a range of applications, and have found that the KPP-LT scheme of Reichl, Wang, et al. (2016) performs best in predicting sea surface temperature cooling under idealized tropical cyclones.

Although wave breaking may be important in modifying the Langmuir turbulence and resulting upper ocean responses, we do not include breaking wave effects in this study because there are no suitable Langmuir turbulence schemes that include breaking wave effects. In Section 3.4, we will discuss possible deficiency of the KPP-LT scheme, which has been developed using idealized Langmuir turbulence LES without accounting for breaking wave effects.

It has been suggested that sea sprays can significantly modify the drag coefficient in high winds (e.g., Hsu et al., 2017; Zijlema et al., 2012). The spray effect is (implicitly) accounted for in this study because the drag coefficient used in this study has been obtained based on the observed upper ocean currents (Zhou et al., 2022).

Finally, Zhou (2022) has conducted the same upper ocean simulations as in this study but including the other surface wave effects on upper ocean currents (the air-sea momentum flux budget, the Stokes advection, the Coriolis-Stokes force, the Stokes-vortex or Stokes shear force). The study shows that these surface wave effects are secondary compared to the dominant effect of the sea-state-dependent Langmuir turbulence. Therefore, they are not included in this study.

3. Results and Discussion

3.1. Wind and Wave Fields

In Figure 4, the results of the 10-m wind speed (top row), the significant wave height (second row), the surface stokes drift (third row), and the surface layer averaged turbulent Langmuir number (bottom row) are presented for 5 TCs at the time when the storm center was closest to the floats (t_0 in Table 1). The horizontal scale is identical in all figures. All these results are presented for Experiment C. The significant wave height and the surface stokes drift slightly vary with different experiments, but the differences are negligibly small (not shown).

The wind fields show that the size of storm varies significantly at the time of the observations; Megi is very small and Ike is very large, in particular. They also show that Megi and Frances are stronger storms. In general, the significant wave height and the surface Stokes drift are larger and the Langmuir number is lower on the right hand side of each TC. These spatial distributions of Langmuir number are generally consistent with those found under idealized storms (Reichl, Ginis, et al., 2016).

3.2. Mixed Layer Turbulence

In this subsection we focus on the Lagrangian float observations of the mixed layer turbulence. Specifically, we investigate the mixed layer averaged (or bulk) vertical velocity variances (VVV), denoted by $\langle w'^2 \rangle$. This quantity is commonly used to quantify the mixed layer turbulence intensity and its enhancement due to the Langmuir turbulence (Harcourt & D'Asaro, 2008; Rabe et al., 2015; Reichl, Wang et al., 2016; Van Roekel et al., 2012). Furthermore, this quantity is often related to the enhancement factor of the turbulent eddy viscosity in mixed layer turbulence models (including the KPP).

Reichl, Wang, et al. (2016) found that the enhancement of the normalized VVV, $\langle w'^2 \rangle / u_*^2$, due to the Langmuir turbulence in LES model simulations under idealized TC is, on average, consistent with the parameterization developed by Van Roekel et al. (2012),

$$\langle w'^2 \rangle / u_*^2 = 0.6\left[1 + (1.5\mathrm{La}_{\mathrm{SL}\theta'})^{-2} + (5.4\mathrm{La}_{\mathrm{SL}\theta'})^{-4}\right], \quad (5)$$

where $\mathrm{La}_{\mathrm{SL}\theta'}$ is the surface layer averaged turbulent Langmuir number defined in Equation 4 (Figure 5b), although this parameterization was originally developed for moderate wind (non-TC) conditions. We first examine whether

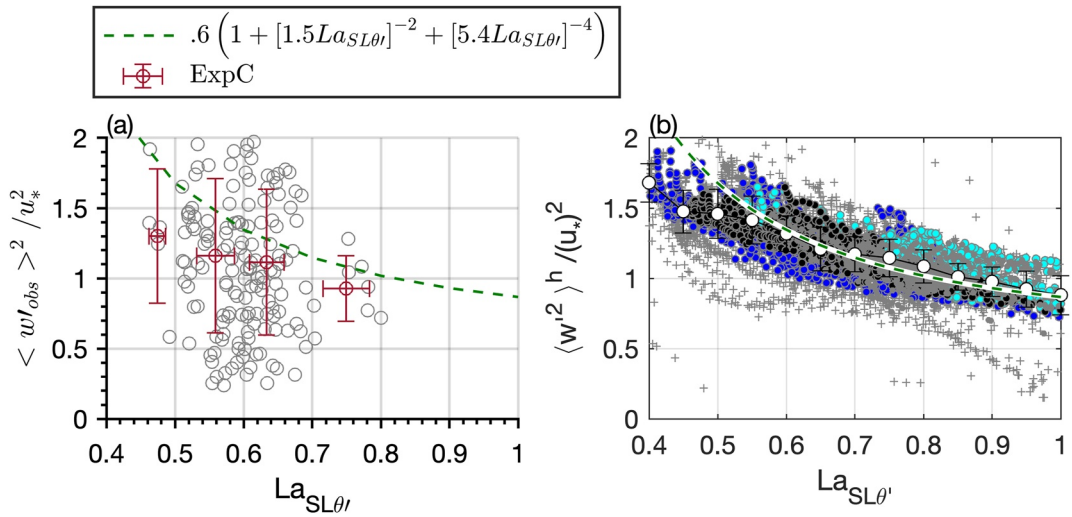

Figure 5. (a) Normalized mixed layer–averaged vertical velocity variance estimates $\langle w'^2\rangle/u_*^2$ ($\langle\langle w'^2\rangle$ from observations and u_*^2 from MOM6 model) are plotted against the surface layer averaged turbulent Langmuir number $La_{SL\theta'}$ (from MOM6 model). Gray circles correspond to $La_{SL\theta'}$ estimated from Experiment (c) Bin averages (every 0.1 increment of $La_{SL\theta'}$) with error bars are shown by red circles, and horizontal bars show standard deviations. (b) Figure 10 from Reichl, Wang et al. (2016). Normalized mixed layer–averaged vertical velocity variance values from LES simulations under idealized TC are plotted against the surface layer averaged turbulent Langmuir number $La_{SL\theta'}$. White circles with vertical bars are bin averages (every 0.05 increment of $La_{SL\theta'}$) with standard deviations. Different symbols/colors indicate different locations relative to the storm center. Detailed description can be found in Reichl, Wang et al. (2016). In both panels, the dashed green lines show the parameterization by Van Roekel et al. (2012).

the observed bulk VVV values in this study, obtained from 12 Lagrangian floats deployed under 4 TCs (Table 1), follow this same parameterization.

Figure 5a shows all the observed normalized VVV values, $\langle w'^2\rangle/u_*^2$, against the surface layer averaged turbulent Langmuir number $La_{SL\theta'}$, which is calculated from the model output (Experiment C). The data are then bin averaged for every 0.1 increment of $La_{SL\theta'}$. In general, the bin-averaged results of normalized bulk VVV are roughly consistent with the previous parameterization by Van Roekel et al. (2012) (green dashed line). Although the data tend to be lower than the parameterization, the vertical error bars (95% confidence) mostly overlap the parameterization. The bottom end of the error bar is always larger than 0.6, that is, the Langmuir turbulence always enhances the VVV relative to the shear only value. Furthermore, the observed enhancement of normalized VVV increases with decreasing Langmuir number as predicted by previous LES studies (Reichl, Wang, et al., 2016; Van Roekel et al., 2012). Our results are certainly not sufficient to validate or invalidate the parameterization by Van Roekel et al. (2012) in TC conditions. In fact, our results tend to be lower than the parameterization by Van Roekel et al. (2012) and suggest that a different parameterization may be needed for TC conditions. However, developing a new parameterization would require substantially more observational data than those in this study.

Reichl, Wang, et al. (2016) found that the bin-averaged normalized VVV values from LES simulations under idealized TCs are consistent with the parameterization by Van Roekel et al. (2012) (compare white circles and green dashed line in Figure 5b). However, notice that the individual estimates from LES results (before bin-averaging) show significant scatter above/below the parameterization; our observed bin-averaged results are within the cloud of LES results. Notice also that the bin averaged LES results deviate lower from the parameterization toward the lower end of $La_{SL\theta'}$, which is consistent with the trend of our observations. These results suggest that the normalized VVV under TCs may scale differently from those in lower winds when $La_{SL\theta'}$ is very small.

Next, we compare the observed bulk VVV values with the estimated bulk VVV values from the 3-D ocean model simulations. Unlike the LES used by Rabe et al. (2015), the MOM6 model does not directly resolve the bulk VVV. However, we can indirectly estimate the Langmuir enhanced $\langle w'^2\rangle$ using the model simulated $La_{SL\theta'}$ values and the empirical parameterization (Equation 5).

Figure 6 shows the time series of bulk VVV at each Lagrangian float location from observations (black), and from model simulations with and without the LT enhancement (red and blue). The blue circles indicate bulk VVV

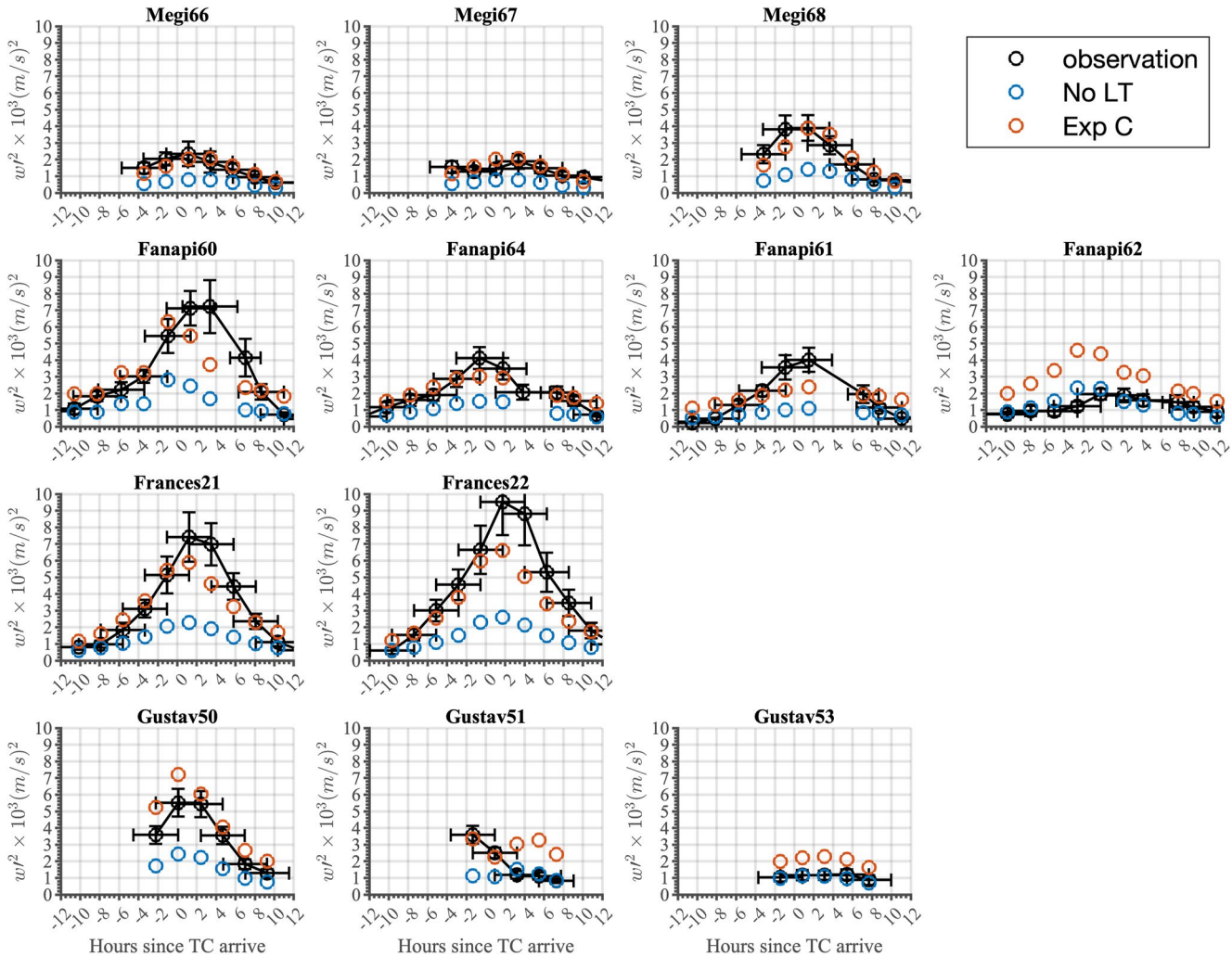

Figure 6. Time series of bulk VVV at each Lagrangian float. Black lines and symbols show observations. Horizontal error bars indicate the averaging time range. Vertical error bars show the 95% confidence level. The model estimates are shown by red (Experiment C) and blue (no LT, shear turbulence only) symbols. Each model estimate is also averaged over the same time range as the corresponding observation.

with shear turbulence only without Langmuir turbulence enhancement, which is equal to $0.6u_*^2$ and is obtained directly from the specified wind forcing fields. Each model result has been averaged over the same time period as the corresponding observational period. These bulk VVV values were obtained from 12 Lagrangian floats deployed, of which 10 floats were deployed on the right of the TC tracks, while 2 floats (Lagrangian float 62 under Fanapi and Lagrangian float 53 under Gustav) were deployed on the left of the TC tracks (Figure 4).

The comparison between the black circle and the blue (or red) circle in Figure 6 is equivalent to the comparison between the black circle and the dashed green line (or constant value of 0.6) in Figure 5, but the comparison is now done without data normalization in Figure 6. The figure clearly shows that the observations are mostly consistent with the model estimates with the Langmuir turbulence enhancement. The estimates with shear turbulence only significantly underestimates VVV.

There are two cases (Fanapi62, Gustav53), where the observed VVV is significantly lower than the model estimates with the Langmuir turbulence enhancement. These are the results from the Lagrangian floats deployed on the left of TC tracks. There is a plausible explanation for this disagreement. Zhou et al. (2022) have found that the drag coefficient is significantly reduced (by a factor of two or so) when the angle between the wind direction and the dominant wave direction exceeds 45°. They have also found that such large wind-wave misalignment is common on the left hand side of TC tracks. Figure 7 shows the misalignment angle $|\psi|$ between dominant surface wave and wind at each Lagrangian float calculated from the WW3 model output. Again, each data point has

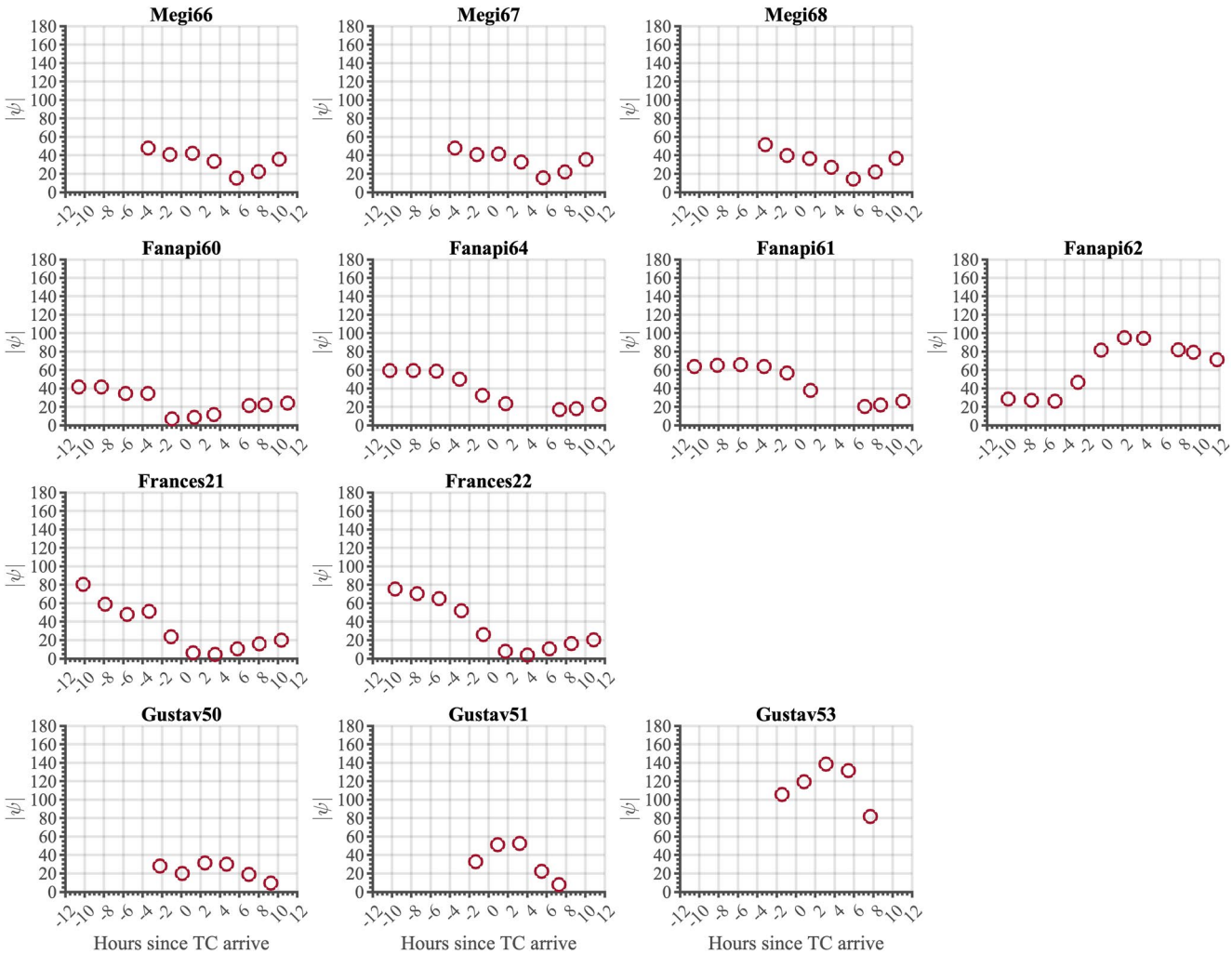

Figure 7. Time series of misalignment angle $|\psi|$ between dominant surface wave and wind at each Lagrangian float from Experiment C.

been averaged over the same time period as the corresponding observation. The figure clearly shows that large misalignment angle (90° or larger) occurred at the two Lagrangian floats on the left hand side (Lagrangian float 62 under Fanapi and 53 under Gustav). In fact, if we reduce our wind stress (and the corresponding VVV estimate) by a factor of 2 at these two float locations, agreement between the observations and the model estimates with the Langmuir turbulence improves significantly (not shown). Note, however, that the wind-wave misalignment is not large but the observed VVV is already low before the storm arrives at the Fanapi62 float. Note also that the wind-wave misalignment is quite large (exceeding 60°) before the storm arrives at a few other floats but the observed VVV is not low. These suggest that the reduced wind stress by wind-wave misalignment may not be the only physical process responsible for modifying the VVV.

In summary, our VVV observations show a clear evidence of enhanced mixed layer turbulence due to the Langmuir turbulence. The enhancement increases with decreasing turbulent Langmuir number and is roughly consistent with the previous LES studies and the parameterization by Van Roekel et al. (2012). Our observations of the reduced VVV on the left of the storm track are consistent with the reduced drag coefficient due to misalignment between dominant surface waves and wind, as found by Zhou et al. (2022).

3.3. Near Surface Eulerian Current Profiles

Since the previous LES studies show that the Langmuir turbulence also impacts the upper ocean current profiles (Reichl, Wang, et al., 2016), we next compare the near surface profiles of wind driven currents between the

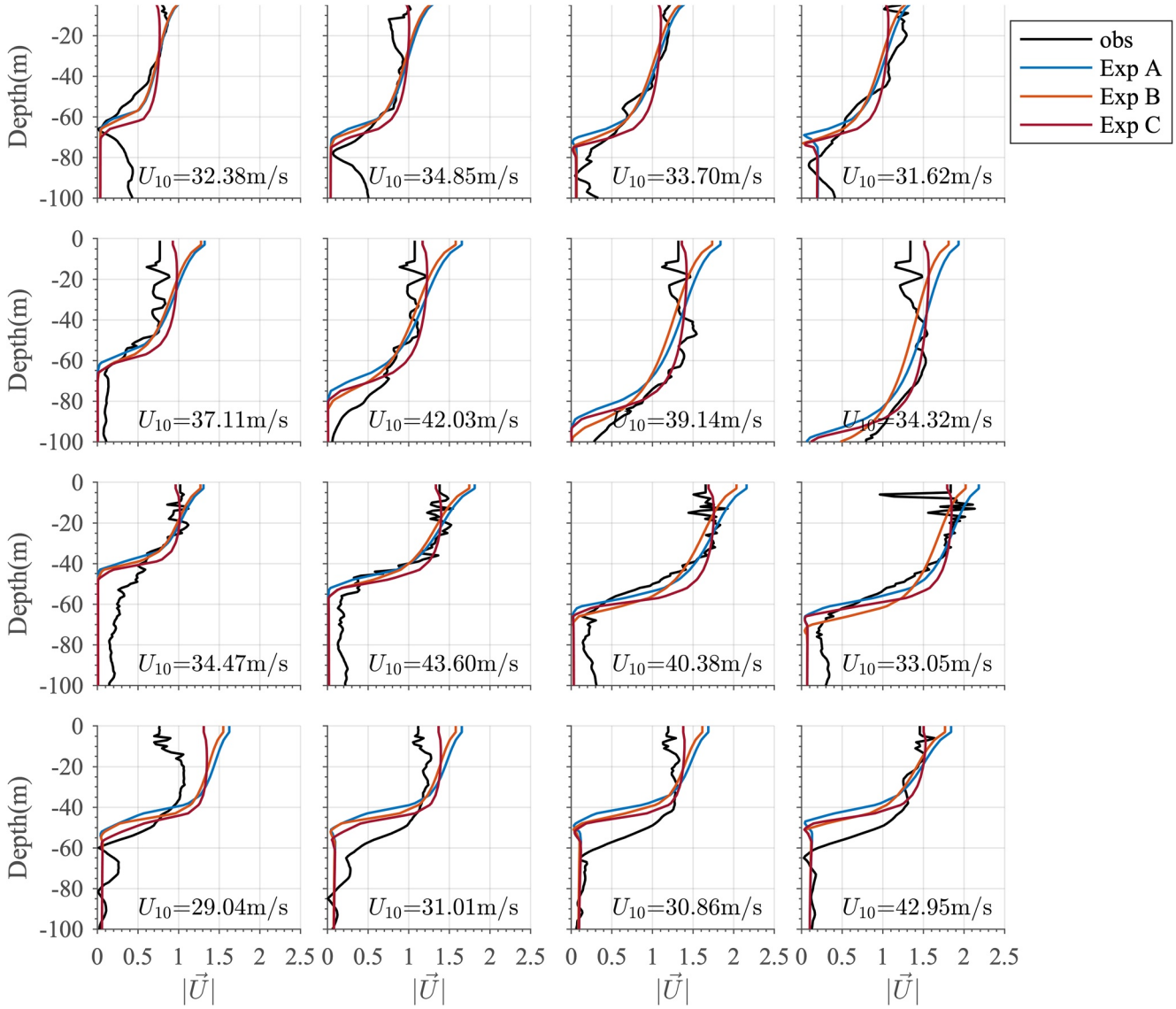

Figure 8. Vertical profiles of magnitude of wind driven currents at 2 hr prior to arrival time of TC (left column), at arrival time of TC (second column), 2 hr after arrival time of TC (third column) and 4 hr after arrival time of TC (right column), observed by EM-APEX float 4907 under Typhoon Fanapi (first row), EM-APEX float 1633 under Hurricane Frances (second row), EM-APEX float 3763 under Hurricane Gustav (third row), and EM-APEX float 3766 under Hurricane Ike (bottom row), are compared with model predictions. Wind Speed (U_{10}) is labeled.

EM-APEX float observations and the model results. The tidal currents and background currents have been removed from the measured currents. The time evolution of vertical wind-driven current profiles are shown in Figure 8 for four floats, from hours −2 to 4 relative to t_0, when the wind forcing was strong. Here, for each storm we have chosen one float that experienced the strongest wind forcing. The result of Megi is not shown since it lacks near surface current data. We immediately notice that the model results are split into two groups. While the model results with the KPP-LT (sea state-dependent Langmuir turbulence) show almost uniform current magnitude in the mixed layer, the results with the KPP-ST (shear only turbulence) and KPP-iLT (sea state-independent Langmuir turbulence) mixing schemes show much stronger near surface current shear and much larger surface current magnitude. These model results are consistent with those under idealized storms (Reichl, Ginis, et al., 2016) and clearly confirms that the KPP-LT homogenizes and reduces the upper ocean current due to enhanced vertical mixing, resulting from the enhancement factor to the eddy viscosity.

The float observations are generally more consistent with the model results with the KPP-LT. In particular, the observations also show weak near surface current shear that is more consistent with the model results with the

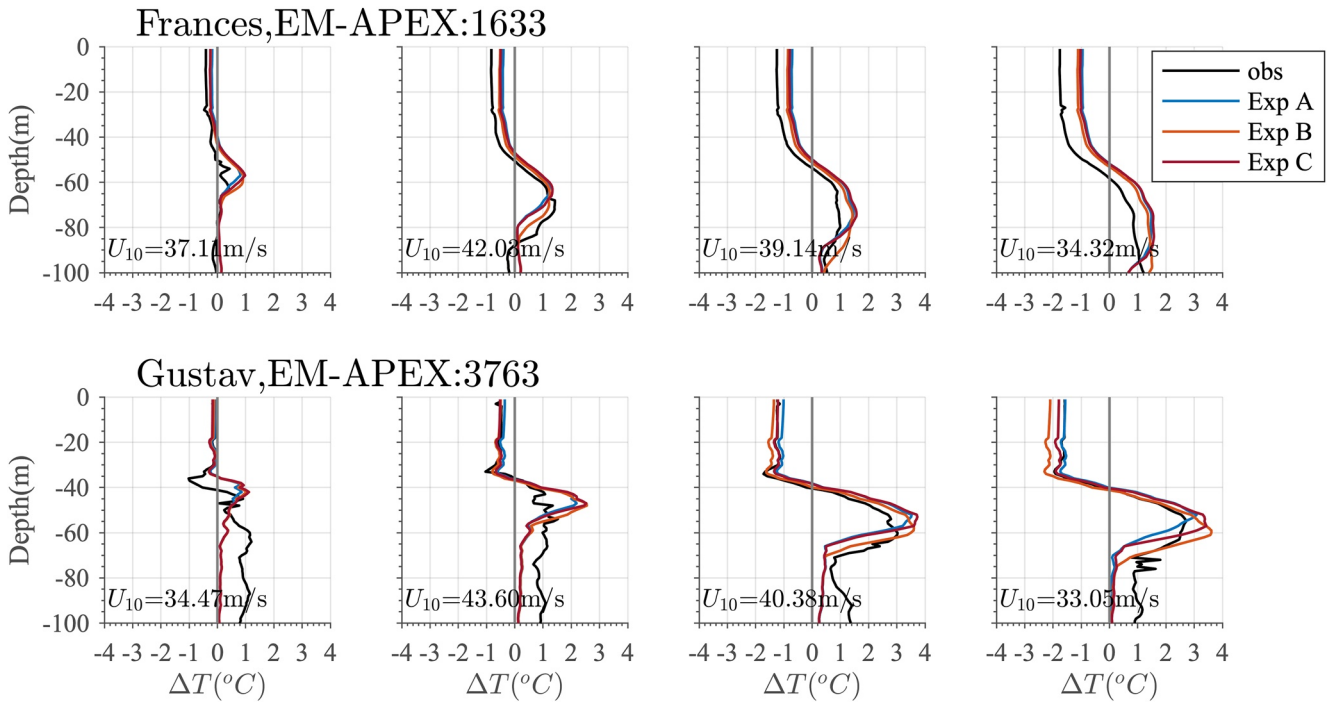

Figure 9. Vertical profiles of temperature anomaly ΔT at 2 hr prior to arrival time of TC (left column), arrival time of TC (second column), 2 hr after arrival time of TC (third column) and 4 hr after arrival time (right column) of TC observed by EM-APEX float 1633 under Hurricane Frances (top row) and EM-APEX float 3763 under Hurricane Gustav (bottom row), are compared with model predictions. Wind Speed (U_{10}) is labeled.

KPP-LT. The shear-driven mixing scheme (KPP-ST) and the implicit Langmuir turbulence (KPP-iLT) significantly overestimates the near surface current shear.

In summary, our float observations of the near surface current provide another strong evidence that the upper ocean turbulence is enhanced by the Langmuir turbulence. Our analyses suggest that accurate predictions of near surface current profiles require a mixing scheme that explicitly includes enhancement by the Langmuir turbulence.

3.4. Temperature and Mixed Layer Depth

In this subsection, we compare temperature and mixed layer depth between model simulations and observations made by EM-APEX floats. The upper ocean cooling $\langle \Delta T \rangle$ is defined as temperature anomaly ΔT averaged over the upper 20 m, and the temperature anomaly ΔT refers to the difference from the initial temperature. The mixed layer depth is defined following Blair et al. (2017) as the depth of the deepest layer where the difference between the temperature of that layer and the SST is $\leq 0.5°C$. The mixed layer depth deepening ΔMLD is defined as the difference from the initial mixed layer depth. The results under Ike are excluded from the analysis since EM-APEX float 3766 encountered a water column containing near coastal fresher water during the deployment, and our simulations using a horizontally homogeneous initial condition may not be accurate.

Two examples of the vertical profiles of temperature anomaly ΔT at -2, 0, 2, and 4 hr after arrival time of TC are presented in Figure 9. The results under Megi and Fanapi are not shown since they lack temperature measurements in upper 30 m most of the time. The simulated upper ocean temperature cooling is roughly consistent with observations under Gustav, but the model underestimates cooling under Frances. (We will discuss the model underestimation of cooling in more detail below).

As discussed earlier, the observed bulk VVV values are significantly lower than the model predictions on the left hand side of the storm track. We suspect this is because the drag coefficient is reduced in the presence of dominant waves misaligned from wind, but the wind stress used in the model has not been reduced.

Here, we present another possible evidence of the reduced drag coefficient on the left of the storm track. The top row of Figure 10 shows time series of misalignment angle between wind and dominant waves at two EM-APEX

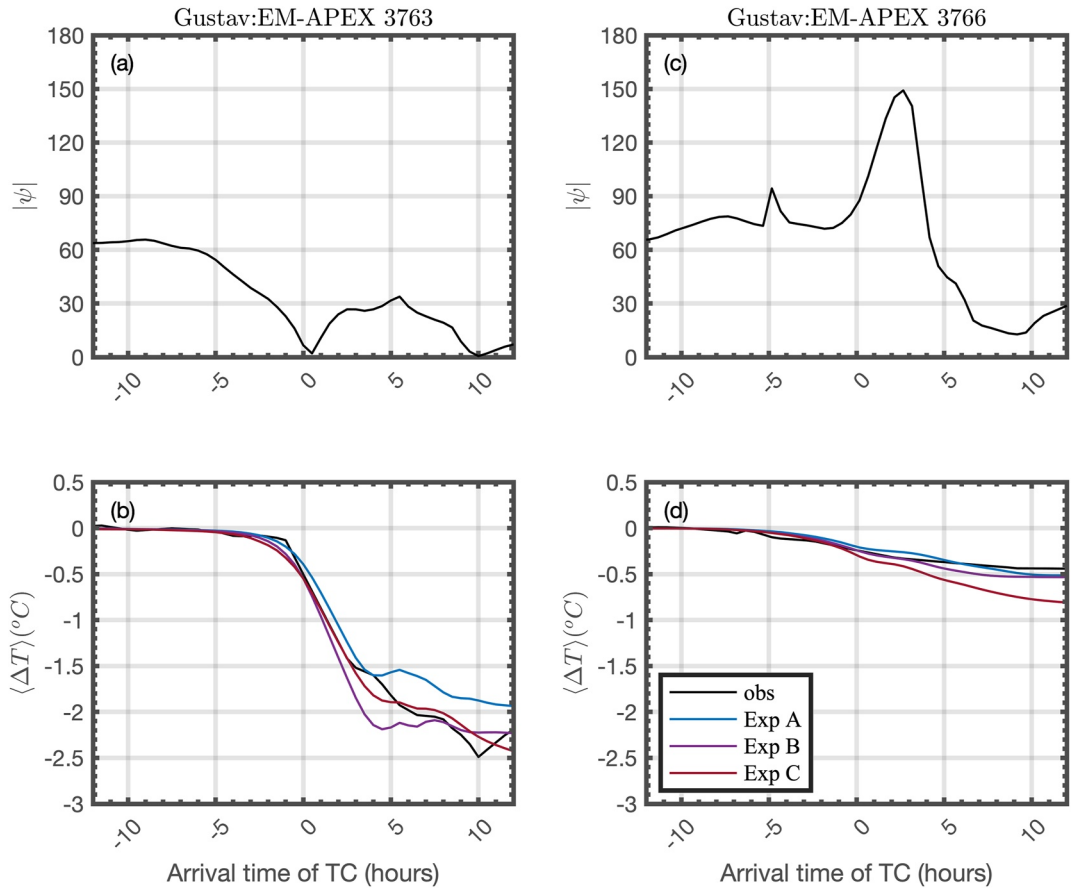

Figure 10. Time series of misalignment angle (ψ) between dominant surface wave and wind (top row) and upper ocean cooling $\langle \Delta T \rangle$ (bottom row) at EM-APEX float 3763 (left) and 3766 (right).

floats under Gustav. Float 3763 was located on the right hand side of the storm track where wind and dominant waves were more aligned during the time of interest (from −2 to 4 hr) (panel a in Figure 10). Float 3766 was on the left hand side of the storm track, where large misalignment occurred (panel c in Figure 10). The model simulation of the upper ocean cooling with the KPP-LT mixing scheme (brown line) is quite consistent with the observation (black line) at Float 3763 (panel b in Figure 10). However, the simulation with the KPP-LT (brown line) significantly overestimates the observation (black line) at Float 3766 (panel d in Figure 10). These results again suggest that the upper ocean cooling on the left of the storm track is overestimated by the model because the drag coefficient is reduced due to misaligned dominant waves but the wind stress in the model has not been reduced.

We next perform statistical analyses to investigate how the observed SST cooling and mixed layer deepening compare with the model predictions in 3 different experiments, using all available EM-APEX observations on the right hand side of storm tracks. (We exclude the data on the left hand side because we suspect they may be affected by the reduced drag coefficient as discussed earlier.) Figure 11 compares observed upper ocean cooling $\langle \Delta T \rangle$ with the model predictions. In this analysis, we have utilized 20 data samples from Fanapi, 89 data samples from Frances and 26 data samples from Gustav.

In panel (a) with the KPP-ST, the fitted regression (red line) with slope 0.64 suggests that the KPP-ST significantly underestimates the upper ocean cooling. When we introduce the Langmuir turbulence the regression slope increases, and the KPP-iLT with slope 0.78 (panel b) performs better than the KPP-LT with slope 0.70 (panel c). However, the model results still underestimate cooling.

We also make a statistical analysis of the mixed layer deepening ΔMLD in Figure 12. In order to focus on initial mixed layer deepening, we have excluded data that are influenced by shallowing mixed layer due to upwelling after the TC has passed. It includes 67 data samples under Frances and 19 data samples under Gustav. Figure 12

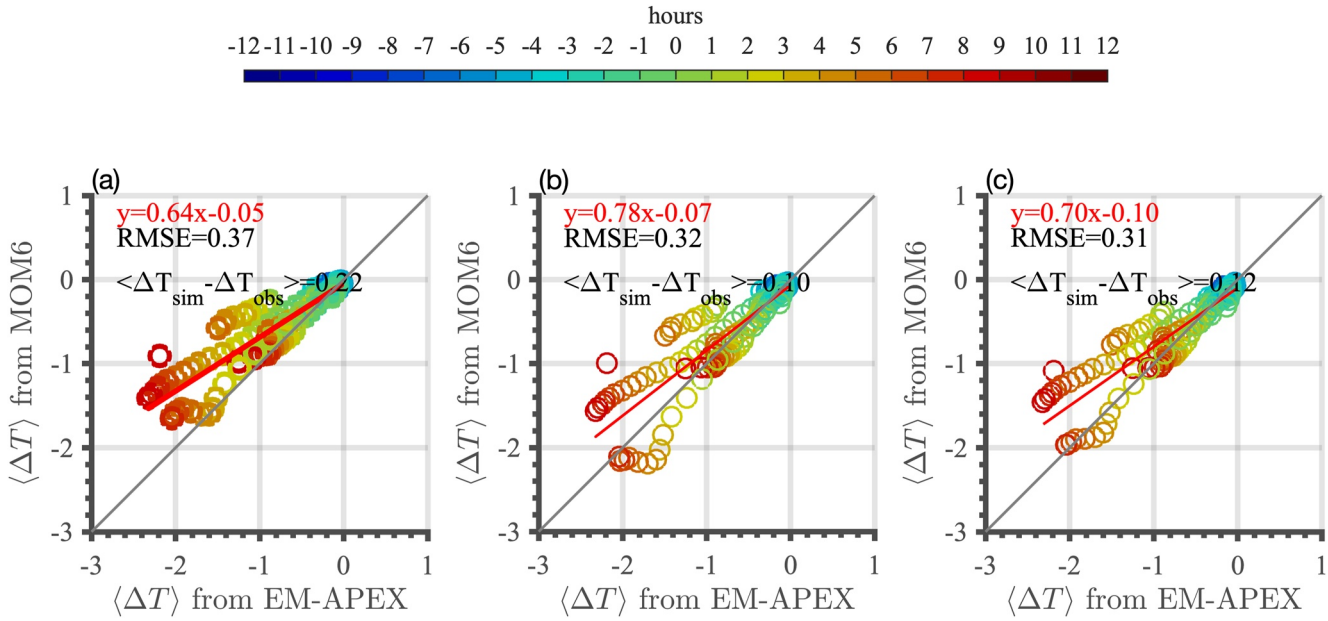

Figure 11. Comparison of observed and modeled upper ocean cooling $\langle \Delta T \rangle$ (in degrees) from Experiment A (a), Experiment B (b), Experiment C (c). The color indicates the time relative to the time of TC arrival. The red line is a fitted linear regression and its slope and offset are labeled. The root mean square error and the mean bias are also labeled.

again suggests that the KPP-ST (panel a) significantly underestimates the mixed layer deepening, with slope 0.63 of the regression line. Including the Langmuir turbulence increases the slope, and the KPP-iLT with slope 0.73 (panel b) performs better than the KPP-LT with slope 0.68 (panel c). But, the models still underestimate deepening.

We have also repeated the same statistical analyses including the observational data on the left hand side. As expected, the regression slope increases slightly (by about 0.02) and the model results agree slightly better with the observations in all cases. However, we suspect that this improvement is mainly because the overestimation of wind stress cancels the underestimation of cooling/deepening on the left hand side.

In summary, the model with the shear only turbulence (KPP-ST scheme) significantly underestimates both upper ocean cooling and mixed layer deepening. Including the Langmuir turbulence (KPP-iLT, KPP-LT) enhances

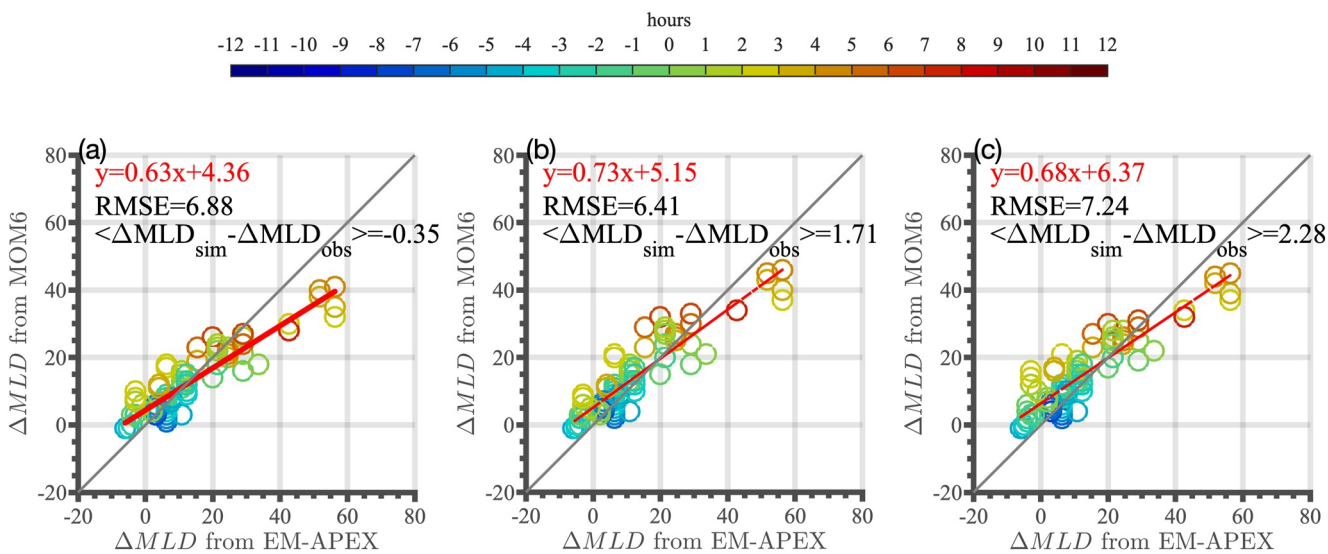

Figure 12. Same as Figure 11, but for mixed layer deepening ΔMLD (in m).

these processes as expected. However, all models, even with the Langmuir turbulence, underestimate the upper ocean cooling and mixed layer deepening by 20%–30%.

3.5. Discussion on Model Performance

In this subsection we consider reasons why the model underestimates the upper ocean cooling and mixed layer deepening even if the enhanced mixing by Langmuir turbulence is included in the model (KPP-iLT or KPP-LT). These processes occur mainly because strong TC wind forcing enhances the upper ocean turbulence and mixing. Therefore, the model underprediction is likely due to underestimation of the applied wind stress, underprediction of the upper ocean mixing (by KPP-iLT or KPP-LT), or both. Since our wind stress applied to the model has been carefully constrained, at least on average over the five storms, we do not think our statistical analyses of mixed layer deepening and cooling, which involve combining all observations, are significantly affected by inaccuracy of the applied wind stress. We suspect that the KPP-iLT and KPP-LT mixing schemes, even with the Langmuir turbulence enhancement, still underestimate upper ocean mixing in realistic oceanic conditions under TCs.

As explained earlier, our KPP schemes have been tuned to reproduce the LES results of the upper ocean cooling and mixed layer deepening under TCs, based on an average over a large number of LES results (Reichl, Wang, et al., 2016). Therefore, there are two possible reasons why our KPP schemes underestimate the mixed layer cooling and deepening. First, the KPP schemes could have shortcomings, such as inadequate representation of entrainment fluxes. Furthermore, the KPP schemes have fewer degrees of freedom than an LES and might not faithfully represent the upper ocean turbulence across a wide range of wind-wave conditions under TCs. It may be necessary to improve the core physics of the KPP model for TC applications. Second, it is possible that the LES itself underestimates upper ocean mixing in realistic oceanic conditions under TCs. Although the first reason is certainly possible, we suspect that the second reason is more likely responsible for the overall KPP underestimation of mixed layer cooling and deepening.

In fact, the LES used in Reichl, Wang, et al. (2016) is highly idealized and may not include all relevant physics. In particular, it does not include the effect of surface breaking waves. Although direct impacts of breaking waves are confined in a relatively shallow surface layer, the combined effects of breaking waves and Langmuir turbulence may penetrate throughout the boundary layer and enhance mixing (Sullivan et al., 2007). We speculate that one likely LES shortcoming is the omission of breaking wave effects.

In this study we do not attempt to evaluate performances of other mixing schemes because every mixing scheme contains tuning parameters, allowing them to be tuned to match any observations or LES results. However, it is expected that any mixing scheme that has been tuned to the same set of LES results used in Reichl, Ginis, et al. (2016) also underestimates the upper ocean cooling and mixed layer deepening in realistic oceanic conditions.

Finally, it is somewhat surprising that the simpler and less accurate KPP-iLT produces more consistent predictions of mixed layer deepening and cooling than the KPP-LT (Figures 11 and 12). We do not think these results suggest that the KPP-iLT is superior to the KPP-LT. Instead, we speculate that the two models give different results because the KPP-LT reproduces the LES results (which underestimate the mixed layer cooling/deepening) more faithfully than the KPP-iLT does.

4. Concluding Remarks

In this study upper ocean responses under tropical cyclones have been investigated by combining field observational data and numerical simulations using a coupled ocean-wave (MOM6-WW3) model. The observational data include vertical profiles of currents, temperature and salinity from the EM-APEX floats and the mixed layer averaged (bulk) vertical velocity variance from the Lagrangian floats. The model simulations are forced by wind stress fields that have been carefully constrained on average (Zhou et al., 2022), but ignore a decrease in stress when the wind and waves are misaligned.

The comparison between the observations and the model simulations presents two strong evidences of enhanced mixing due to the Langmuir turbulence. First, the observed normalized bulk vertical velocity variance, $\langle w'^2 \rangle / u_*^2$, is significantly enhanced relative to the value expected for shear-only turbulence. The enhancement increases as the surface layer averaged turbulent Langmuir number $La_{SL\theta'}$ decreases, which is consistent with the previous LES modeling results (Reichl, Wang, et al., 2016) under TCs. Although the previous observational study (Rabe

et al., 2015) also reported enhanced turbulence, this is the first time the correlation between the normalized bulk vertical velocity variance and the turbulent Langmuir number has been confirmed under TCs. It is also noteworthy that the observed correlation is roughly consistent with the parameterization by Van Roekel et al. (2012) and observations by D'Asaro, Black, et al. (2014) and D'Asaro, Thomson, et al. (2014) at lower wind speeds. Second, the observed current profiles in the upper 20 m are weakly sheared, and are consistent with the model simulations with the KPP-LT mixing scheme that includes explicit sea state-dependent Langmuir turbulence enhancement. The simulations with the KPP-ST (shear only) or KPP-iLT (with the Langmuir turbulence but without its sea-state dependence) significantly overestimate near surface current shear and surface current magnitude. To our knowledge, this is the first time the reduced near-surface current shear by the Langmuir turbulence has been observed in the upper ocean responses under tropical cyclone wind forcing. These results suggest that accurate predictions of upper ocean turbulence and currents require a mixing scheme that explicitly considers the effect of Langmuir turbulence enhancement.

The previous study by Zhou et al. (2022), based on the same observational data set, shows that the drag coefficient is significantly reduced (by a factor of about 2) due to the dominant surface waves misaligned from the wind by more than 45°, and that such misalignment is common on the left hand side of the storm track. The results of this study show two additional evidences of the reduced wind forcing on the left hand side of the track. First, the observed $\langle w'^2 \rangle / u_*^2$ values from the two floats deployed on the left hand side of the track are significantly lower than the model prediction with the KPP-LT. Second, the temperature observations from the two EM-APEX floats (one deployed on the left and the other on the right of the track) under Gustav show that the observed upper ocean cooling is consistent with the model prediction with the KPP-LT on the right, but is significantly less than the model prediction on the left of the track. These two new observations further suggest that the drag coefficient is significantly reduced by the presence of misaligned dominant waves, that is, the drag coefficient strongly depends on sea states. Two recent observational studies also report reduced drag coefficients when wind and dominant waves are misaligned (Chen et al., 2022; Potter et al., 2022). In this study we have not attempted to introduce a sea state-dependent drag coefficient parameterization because existing observations are too limited to constrain the sea state dependence with reasonable confidence. Nevertheless, the combined results from Zhou et al. (2022) and from this study clearly suggest that such an effort is needed for accurate predictions of upper ocean responses under tropical cyclones.

Another important finding is that the model simulations underestimate the upper ocean cooling and mixed layer deepening by 20%–30% even with the mixing schemes (KPP-iLT, KPP-LT) that include the Langmuir turbulence enhancement. Since our KPP mixing schemes have been carefully tuned to reproduce the LES results, we suspect that the model underestimation of mixed layer cooling/deepening may indicate deficiency of the idealized LES results that do not include all relevant physical processes, such as surface breaking wave effects.

In summary, this study confirms the importance of surface waves for ocean cooling and thus TC intensity, through both Cd and LT effects, but caution that existing mixing models may still underestimate upper ocean cooling and mixed layer deepening.

Acknowledgments
We acknowledge support of the National Science Foundation (Physical Oceanography) Grant OCE1756164. We also acknowledge high-performance computing support from Cheyenne (https://doi.org/10.5065/D6RX99HX) provided by NCAR's Computational and Information Systems Laboratory, sponsored by the National Science Foundation. IG was supported by a grant from the Ministry of Ocean and Fisheries, Korea, URI Award AWD06003. We thank Aakash Sane for comments on this manuscript. We thank the reviewers for their valuable comments and suggestions, which have helped us to improve the manuscript. Finally, we acknowledge the contribution (EM-APEX data) of Thomas Sanford. This work would not have been possible without him.

Data Availability Statement

The model simulation and processed float data set in this study can be accessed from the Mendeley data repository https://doi.org/10.17632/tc74d4vk6k.1 (Zhou et al., 2023). The up-to-date working versions of source code of MOM6 and WAVEWATCH III, can be found at Github (NOAA-EMC, 2023; NOAA-GFDL, 2023). The coupled version of coupled MOM6-WWIII code used in this study can be found at Github (Reichl, 2022).

References

Adcroft, A., Anderson, W., Balaji, V., Blanton, C., Bushuk, M., Dufour, C. O., et al., (2019). The GFDL global ocean and sea ice model om4. 0: Model description and simulation features. *Journal of Advances in Modeling Earth Systems*, *11*(10), 3167–3211. https://doi.org/10.1029/2019ms001726

Bender, M. A., & Ginis, I. (2000). Real-case simulations of hurricane–ocean interaction using a high-resolution coupled model: Effects on hurricane intensity. *Monthly Weather Review*, *128*(4), 917–946.

Biswas, M. (2018). *Hurricane weather research and forecasting (HWRF) model: 2018 scientific documentation*. Development Testbed Centre Report.

Blair, A., Ginis, I., Hara, T., & Ulhorn, E. (2017). Impact of Langmuir turbulence on upper ocean response to hurricane Edouard: Model and observations. *Journal of Geophysical Research: Oceans*, *122*(12), 9712–9724. https://doi.org/10.1002/2017JC012956

Bryant, K. M., & Akbar, M. (2016). An exploration of wind stress calculation techniques in hurricane storm surge modeling. *Journal of Marine Science and Engineering*, *4*(3), 58. https://doi.org/10.3390/jmse4030058

Chen, S., Qiao, F., Zhang, J. A., Xue, Y., Ma, H., & Chen, S. (2022). Observed drag coefficient asymmetry in a tropical cyclone. *Journal of Geophysical Research: Oceans*, *127*(9), e2021JC018360. https://doi.org/10.1029/2021jc018360

Chen, X., Ginis, I., & Hara, T. (2020). Impact of shoaling ocean surface waves on wind stress and drag coefficient in coastal waters: 2. Tropical cyclones. *Journal of Geophysical Research: Oceans*, *125*(7), e2020JC016222. https://doi.org/10.1029/2020JC016223

Chih, C.-H., & Wu, C.-C. (2020). Exploratory analysis of upper-ocean heat content and sea surface temperature underlying tropical cyclone rapid intensification in the western north pacific. *Journal of Climate*, *33*(3), 1031–1050. https://doi.org/10.1175/jcli-d-19-0305.1

Craik, A. D., & Leibovich, S. (1976). A rational model for Langmuir circulations. *Journal of Fluid Mechanics*, *73*(3), 401–426. https://doi.org/10.1017/s0022112076001420

D'Asaro, E. (2003). Performance of autonomous Lagrangian floats. *Journal of Atmospheric and Oceanic Technology*, *20*(6), 896–911. https://doi.org/10.1175/1520-0426(2003)020<0896:POALF>2.0.CO;2

D'Asaro, E. (2014). Turbulence in the upper-ocean mixed layer. *Annual Review of Marine Science*, *6*(1), 101–115. https://doi.org/10.1146/annurev-marine-010213-135138

D'Asaro, E. (2015). Surface wave measurements from subsurface floats. *Journal of Atmospheric and Oceanic Technology*, *32*(4), 816–827. https://doi.org/10.1175/JTECH-D-14-00180.1

D'Asaro, E., Black, P. G., Centurioni, L. R., Chang, Y.-T., Chen, S. S., Foster, R. C., et al. (2014). Impact of typhoons on the ocean in the pacific. *Bulletin of the American Meteorological Society*, *95*(9), 1405–1418. https://doi.org/10.1175/BAMS-D-12-00104.1

D'Asaro, E., Black, P., Centurioni, L., Harr, P., Jayne, S., Lin, I.-I., et al. (2011). Typhoon-Ocean interaction in the western north pacific: Part 1. *Oceanography*, *24*, 24–31.

D'Asaro, E., & Dairiki, G. T. (1997). Turbulence intensity measurements in a wind-driven mixed layer. *Journal of Physical Oceanography*, *27*(9), 2009–2022. https://doi.org/10.1175/1520-0485(1997)027<2009:TIMIAW>2.0.CO;2

D'Asaro, E., Farmer, D. M., Osse, J. T., & Dairiki, G. T. (1996). A Lagrangian float. *Journal of Atmospheric and Oceanic Technology*, *13*(6), 1230–1246. https://doi.org/10.1175/1520-0426(1996)013<1230:alf>2.0.co;2

D'Asaro, E., Thomson, J., Shcherbina, A. Y., Harcourt, R. R., Cronin, M. F., Hemer, M. A., & Fox-Kemper, B. (2014). Quantifying upper ocean turbulence driven by surface waves. *Geophysical Research Letters*, *41*(1), 102–107. https://doi.org/10.1002/2013GL058193

Donelan, M. A., Curcic, M., Chen, S. S., & Magnusson, A. K. (2012). Modeling waves and wind stress. *Journal of Geophysical Research*, *117*(C11). https://doi.org/10.1029/2011JC007787

Emanuel, K. A. (1991). The theory of hurricanes. *Annual Review of Fluid Mechanics*, *23*(1), 179–196. https://doi.org/10.1146/annurev.fl.23.010191.001143

Fan, Y., Ginis, I., Hara, T., Wright, C. W., & Walsh, E. J. (2009). Numerical simulations and observations of surface wave fields under an extreme tropical cyclone. *Journal of Physical Oceanography*, *39*(9), 2097–2116. https://doi.org/10.1175/2009jpo4224.1

Fan, Y., & Griffies, S. M. (2014). Impacts of parameterized Langmuir turbulence and nonbreaking wave mixing in global climate simulations. *Journal of Climate*, *27*(12), 4752–4775. https://doi.org/10.1175/jcli-d-13-00583.1

Ginis, I. (2002). Tropical cyclone-ocean interactions. *Advances in Fluid Mechanics*, *33*, 83–114.

Ginis, I., Bender, M., Thomas, B., Morin, M., Tallapragada, V., & Soloviev, A. (2015). A new drag coefficient formulation and its impact on the GFDL and HWRF hurricane model predictions. In *19th conference on air-sea interaction* (Vol. 8).

Harcourt, R. R., & D'Asaro, E. A. (2008). Large-eddy simulation of Langmuir turbulence in pure wind seas. *Journal of Physical Oceanography*, *38*(7), 1542–1562. https://doi.org/10.1175/2007jpo3842.1

Holthuijsen, L. H., Powell, M. D., & Pietrzak, J. D. (2012). Wind and waves in extreme hurricanes. *Journal of Geophysical Research*, *117*(C9). https://doi.org/10.1029/2012JC007983

Hsu, J.-Y., Lien, R.-C., D'Asaro, E. A., & Sanford, T. B. (2017). Estimates of surface wind stress and drag coefficients in typhoon Megi. *Journal of Physical Oceanography*, *47*(3), 545–565. https://doi.org/10.1175/JPO-D-16-0069.1

Hsu, J.-Y., Lien, R.-C., D'Asaro, E. A., & Sanford, T. B. (2019). Scaling of drag coefficients under five tropical cyclones. *Geophysical Research Letters*, *46*(6), 3349–3358. https://doi.org/10.1029/2018GL081574

Hwang, P. A., Fan, Y., Ocampo-Torres, F. J., & García-Nava, H. (2017). Ocean surface wave spectra inside tropical cyclones. *Journal of Physical Oceanography*, *47*(10), 2393–2417. https://doi.org/10.1175/jpo-d-17-0066.1

Kukulka, T., Plueddemann, A. J., Trowbridge, J. H., & Sullivan, P. P. (2009). Significance of Langmuir circulation in upper ocean mixing: Comparison of observations and simulations. *Geophysical Research Letters*, *36*(10), L10603. https://doi.org/10.1029/2009gl037620

Large, W. G., McWilliams, J. C., & Doney, S. C. (1994). Oceanic vertical mixing: A review and a model with a nonlocal boundary layer parameterization. *Reviews of Geophysics*, *32*(4), 363–403. https://doi.org/10.1029/94rg01872

Li, Q., Reichl, B. G., Fox-Kemper, B., Adcroft, A. J., Belcher, S. E., Danabasoglu, G., et al. (2019). Comparing ocean surface boundary vertical mixing schemes including Langmuir turbulence. *Journal of Advances in Modeling Earth Systems*, *11*(11), 3545–3592. https://doi.org/10.1029/2019ms001810

Li, Q., Webb, A., Fox-Kemper, B., Craig, A., Danabasoglu, G., Large, W. G., & Vertenstein, M. (2016). Langmuir mixing effects on global climate: Wavewatch III in CESM. *Ocean Modelling*, *103*, 145–160. https://doi.org/10.1016/j.ocemod.2015.07.020

Liu, Q., Babanin, A., Fan, Y., Zieger, S., Guan, C., & Moon, I.-J. (2017). Numerical simulations of ocean surface waves under hurricane conditions: Assessment of existing model performance. *Ocean Modelling*, *118*, 73–93. https://doi.org/10.1016/j.ocemod.2017.08.005

McWilliams, J. C., Sullivan, P. P., & Moeng, C.-H. (1997). Langmuir turbulence in the ocean. *Journal of Fluid Mechanics*, *334*, 1–30. https://doi.org/10.1017/s0022112096004375

Moon, I.-J., Ginis, I., Hara, T., Tolman, H. L., Wright, C., & Walsh, E. J. (2003). Numerical simulation of sea surface directional wave spectra under hurricane wind forcing. *Journal of Physical Oceanography*, *33*(8), 1680–1706. https://doi.org/10.1175/2410.1

NOAA-EMC. (2023). Wave watch III [software]. Github. Retrieved https://github.com/NOAA-EMC/WW3/

NOAA-GFDL. (2023). Mom6 [software]. Github. Retrieved https://github.com/NOAA-GFDL/MOM6

Noh, Y., Min, H. S., & Raasch, S. (2004). Large eddy simulation of the ocean mixed layer: The effects of wave breaking and Langmuir circulation. *Journal of Physical Oceanography*, *34*(4), 720–735. https://doi.org/10.1175/1520-0485(2004)034<0720:lesoto>2.0.co;2

Polton, J. A., & Belcher, S. E. (2007). Langmuir turbulence and deeply penetrating jets in an unstratified mixed layer. *Journal of Geophysical Research*, *112*(C9), C09020. https://doi.org/10.1029/2007jc004205

Potter, H., Collins, C. O., & Ortiz-Suslow, D. G. (2022). Pier-based measurements of air-sea momentum fluxes over shoaling waves during Dunex. *Journal of Geophysical Research: Oceans*, *127*(11), e2022JC018801. https://doi.org/10.1029/2022jc018801

Powell, M. D., Vickery, P. J., & Reinhold, T. A. (2003). Reduced drag coefficient for high wind speeds in tropical cyclones. *Nature*, *422*(6929), 279–283. https://doi.org/10.1038/nature01481

Price, J. F. (1981). Upper ocean response to a hurricane. *Journal of Physical Oceanography*, *11*(2), 153–175. https://doi.org/10.1175/1520-0485(1981)011<0153:uortah>2.0.co;2

Rabe, T. J., Kukulka, T., Ginis, I., Hara, T., Reichl, B. G., D'Asaro, E. A., et al. (2015). Langmuir turbulence under hurricane Gustav (2008). *Journal of Physical Oceanography*, *45*(3), 657–677. https://doi.org/10.1175/JPO-D-14-0030.1

Reichl, B. (2022). FMS wave coupling [software]. Github. Retrieved from https://github.com/breichl/FMS_Wave_Coupling

Reichl, B. G., Ginis, I., Hara, T., Thomas, B., Kukulka, T., & Wang, D. (2016). Impact of sea-state-dependent Langmuir turbulence on the ocean response to a tropical cyclone. *Monthly Weather Review*, *144*(12), 4569–4590. https://doi.org/10.1175/mwr-d-16-0074.1

Reichl, B. G., Wang, D., Hara, T., Ginis, I., & Kukulka, T. (2016). Langmuir turbulence parameterization in tropical cyclone conditions. *Journal of Physical Oceanography*, *46*(3), 863–886. https://doi.org/10.1175/JPO-D-15-0106.1

Sanford, T. B., Price, J. F., & Girton, J. B. (2011). Upper-Ocean response to hurricane Frances (2004) observed by profiling EM-APEX floats. *Journal of Physical Oceanography*, *41*(6), 1041–1056. https://doi.org/10.1175/2010JPO4313.1

Sullivan, P. P., McWilliams, J. C., & Melville, W. K. (2007). Surface gravity wave effects in the oceanic boundary layer: Large-eddy simulation with vortex force and stochastic breakers. *Journal of Fluid Mechanics*, *593*, 405–452. https://doi.org/10.1017/s002211200700897x

Sullivan, P. P., Romero, L., McWilliams, J. C., & Melville, W. K. (2012). Transient evolution of Langmuir turbulence in ocean boundary layers driven by hurricane winds and waves. *Journal of Physical Oceanography*, *42*(11), 1959–1980. https://doi.org/10.1175/jpo-d-12-025.1

Tsujino, H., Urakawa, S., Nakano, H., Small, R. J., Kim, W. M., Yeager, S. G., et al. (2018). JRA-55 based surface dataset for driving ocean–sea-ice models (JRA55-do). *Ocean Modelling*, *130*, 79–139. https://doi.org/10.1016/j.ocemod.2018.07.002

Van Roekel, L., Fox-Kemper, B., Sullivan, P., Hamlington, P., & Haney, S. (2012). The form and orientation of Langmuir cells for misaligned winds and waves. *Journal of Geophysical Research*, *117*(C5). https://doi.org/10.1029/2011jc007516

Wang, X., Kukulka, T., & Plueddemann, A. J. (2022). Wind fetch and direction effects on Langmuir turbulence in a coastal ocean. *Journal of Geophysical Research: Oceans*, *127*(5), e2021JC018222. https://doi.org/10.1029/2021jc018222

WW3DG. (2019). User manual and system documentation of WAVEWATCH III version 6.07, The WAVEWATCH III Development Group. Tech. Note 326, NOAA/NWS/NCEP/MMAB, College Park, MD, pp.+ Appendices.

Yablonsky, R. M., & Ginis, I. (2009). Limitation of one-dimensional ocean models for coupled hurricane–ocean model forecasts. *Monthly Weather Review*, *137*(12), 4410–4419. https://doi.org/10.1175/2009mwr2863.1

Zhang, H., Chen, D., Zhou, L., Liu, X., Ding, T., & Zhou, B. (2016). Upper ocean response to typhoon kalmaegi (2014). *Journal of Geophysical Research: Oceans*, *121*(8), 6520–6535. https://doi.org/10.1002/2016jc012064

Zheng, Z., Harcourt, R. R., & D'Asaro, E. A. (2021). Evaluating Monin–Obukhov scaling in the unstable oceanic surface layer. *Journal of Physical Oceanography*, *51*(3), 911–930. https://doi.org/10.1175/jpo-d-20-0201.1

Zhou, X. (2022). *Effects of surface waves on wind stress and upper ocean response under tropical cyclones (Unpublished doctoral dissertation)*. University of Rhode Island.

Zhou, X., Hara, T., Ginis, I., D'Asaro, E., Hsu, J.-Y., & Reichl, B. G. (2022). Drag coefficient and its sea state dependence under tropical cyclones. *Journal of Physical Oceanography*, *52*(7), 1447–1470. https://doi.org/10.1175/jpo-d-21-0246.1

Zhou, X., Hara, T., Ginis, I., D'Asaro, E., & Reichl, B. G. (2023). Evidence of Langmuir mixing effects in the upper ocean layer during tropical cyclones using observations and a coupled wave-ocean model [Dataset]. Mendeley Data, V1. https://doi.org/10.17632/tc74d4vk6k.1

Zijlema, M., Van Vledder, G. P., & Holthuijsen, L. (2012). Bottom friction and wind drag for wave models. *Coastal Engineering*, *65*, 19–26. https://doi.org/10.1016/j.coastaleng.2012.03.002